

Pure spin photocurrent in non-centrosymmetric crystals: bulk spin photovoltaic effect

Haowei Xu¹, Hua Wang¹, Jian Zhou ¹ & Ju Li ^{1,2}✉

Spin current generators are critical components for spintronics-based information processing. In this work, we theoretically and computationally investigate the bulk spin photovoltaic (BSPV) effect for creating DC spin current under light illumination. The only requirement for BSPV is inversion symmetry breaking, thus it applies to a broad range of materials and can be readily integrated with existing semiconductor technologies. The BSPV effect is a cousin of the bulk photovoltaic (BPV) effect, whereby a DC charge current is generated under light. Thanks to the different selection rules on spin and charge currents, a pure spin current can be realized if the system possesses mirror symmetry or inversion-mirror symmetry. The mechanism of BSPV and the role of the electronic relaxation time τ are also elucidated. We apply our theory to several distinct materials, including monolayer transition metal dichalcogenides, anti-ferromagnetic bilayer MnBi_2Te_4 , and the surface of topological crystalline insulator cubic SnTe .

¹Department of Nuclear Science and Engineering, Massachusetts Institute of Technology, Cambridge, MA, USA. ²Department of Materials Science and Engineering, Massachusetts Institute of Technology, Cambridge, MA, USA. ✉email: liju@mit.edu

Present-day electronics, which utilize the charge degree of freedom of electrons, have revolutionized human civilization. Besides charge, spin is another intrinsic freedom of electrons that can be exploited for information processing. Indeed, spintronics^{1,2} is promising for next-generation energy-efficient devices and other novel applications such as quantum computing^{3,4} and neuromorphic computation⁵. One of the core challenges⁶ of spintronics is the generation of a spin current, and particularly, a *pure* spin current without an accompanying charge current. Until now, there have been a few approaches, such as the interconversion between charge and spin currents by (inverse) spin galvanic effect^{7,8} or (inverse) spin Hall effect^{9–12}, and the interconversion between thermal and spin currents by spin Seebeck effect^{13,14} or spin Nernst effect^{15,16}, etc. These approaches all require electrode contact and patterning, and the response time is usually on the order of nanoseconds or longer. In contrast, optical approaches are noncontact, noninvasive, and can enable ultrafast response time on the order of picoseconds and below.

Several optical approaches for generating spin currents have been proposed; however, these approaches typically require special ingredients, such as the breaking of time-reversal symmetry \mathcal{T} by introducing magnetic elements or circularly polarized light (CPL), and/or special device structures. For example, CPL can selectively couple with spin-up and spin-down states in quantum wells¹⁷, or spin-valley locked systems¹⁸, and the imbalanced population of spin-up and spin-down states could lead to a spin photocurrent. In magnetic materials, it has also been proposed that a linearly polarized light (LPL) can generate a spin current with the shift-current mechanism^{19–22}. Alternatively, a spin current can be generated with a mechanism reminiscent of the p–n junction in solar cells^{23–25}, quantum interference^{26,27}, or the nonlinear Drude current²⁸. Although progress has been made, the generation of spin currents under light is still under-explored. In particular, it is highly desirable to introduce new mechanisms applicable to a broader family of materials.

In this work, we propose a mechanism to generate direct current (DC) spin current based on the nonlinear optical (NLO) theory. This mechanism is a cousin of the bulk photovoltaic (BPV) effect^{29,30}, whereby DC charge currents can be generated in a uniform crystal under light illumination. The BPV effect, together with other NLO effects, are under intensive research recently, but thus far the attention is mainly on the charge current, while the spin current has long been neglected. Certainly, when the charge flows under light, the spin associated with the carriers are moving as well, which is a spin current. In some situations, the charge current vanishes due to symmetry, but this does not indicate that the carriers are frozen in materials. Indeed, the carriers generally still move under above-bandgap light illumination, which leads to a nonzero pure spin current. A generic picture here is that electrons with opposite (or at least different) spin polarizations travel in the opposite directions so that the net charge current is zero, while the net spin current is nonzero (Fig. 1). We name this effect the bulk spin photovoltaic (BSPV) effect. Here the “voltaic” is defined as $V_{\uparrow\downarrow} \equiv (\mu_{\uparrow} - \mu_{\downarrow})/(-e)$, which is the difference between the chemical potential of spin-up (μ_{\uparrow}) and spin-down (μ_{\downarrow}) electrons. This should be compared with the BPV voltage, which may be defined as $U \equiv (\mu_{\uparrow} + \mu_{\downarrow})/(-2e)$. Similar to the BPV voltage U , the BSPV voltage $V_{\uparrow\downarrow}$ will not be limited by the bandgap of the material, and the currents will not be limited by the Shockley–Queisser limit.

In the following, we first introduce a unified theory on NLO spin (BSPV) and charge (BPV) currents generation. Then, combining theoretical analysis and ab initio calculations, we elucidate some prominent features of the BSPV. Notably, the only requirements for BSPV are (a) above-direct-bandgap light

illumination, and (b) the breaking of inversion symmetry \mathcal{P} , regardless of \mathcal{T} . There are no need for any special ingredients such as magnetic materials, special device structures (quantum wells, junctions, etc.), the interference between two pulses, or specific light wavelength or polarization. Hence, BSPV has great convenience in practice and can be readily integrated with existing semiconductor technologies^{31,32}. These advantages, together with the flexibilities of optical approaches (dynamic spatial addressability, tunable intensity, wavelength, polarization, etc.), provide a large playground to be explored. These results are useful not only for generating spin currents but also for material characterization and sensing. Many applications that are not envisaged before may become possible. In addition, we also clarify the lattice symmetry requirements for the generation of pure spin current, and the mechanisms (shift- and/or injection-like) for spin current generation under different symmetry conditions and light polarizations.

Results

General theory and symmetry analysis. The NLO charge or spin current under light with frequency ω can be expressed as

$$J^{a,s^i} = \sum_{\Omega=\pm\omega} \sigma_{bc}^{a,s^i}(0; \Omega, -\Omega) E^b(\Omega) E^c(-\Omega) \quad (1)$$

Here $E(\omega)$ is the Fourier component of the electric field at angular frequency ω . σ_{bc}^{a,s^i} is the NLO conductivity, with a, b, c as Cartesian indices. a indicates the direction of the current, while b and c are the polarization of the optical electric field. s^i with $i = x, y, z$ is the spin polarization, while s^0 represents charge current. The spin and charge are in the unit of angular momentum $\frac{\hbar}{2}$ and electron charge e , respectively. To directly compare the values of the charge and spin current conductivity, we divide the spin current conductivity by a factor of $\frac{\hbar}{2e}$ ³³. Equation (1) suggests that the $+\omega$ and $-\omega$ components of the electric field are combined, and a direct current is generated. We derived the formula for σ_{bc}^{a,s^i} from quadratic response theory^{30,34} (see Supplementary Information). Within the independent particle approximation, the conductivity can be expressed as

$$\begin{aligned} & \sigma_{bc}^{a,s^i}(0; \omega, -\omega) \\ &= -\frac{e^2}{\hbar^2 \omega^2} \int \frac{d\mathbf{k}}{(2\pi)^3} \sum_{mnl} \frac{f_{lm} v_{lm}^b}{\omega_{ml} - \omega + i/\tau} \left(\frac{j_{mn}^{a,s^i} v_{nl}^c}{\omega_{mn} + i/\tau} - \frac{v_{mn}^c j_{nl}^{a,s^i}}{\omega_{nl} + i/\tau} \right) \end{aligned} \quad (2)$$

Here the explicit \mathbf{k} -dependence of the quantities are omitted. $f_{lm} = f_l - f_m$ and $\omega_{lm} = \omega_l - \omega_m$ are the difference of occupation number and band energy between bands l and m . $v_{nl} \equiv \langle n | \hat{v} | l \rangle$ is the velocity matrix element, while τ is the carrier lifetime, and is set to be 0.2 ps uniformly in this paper. The symmetric real and asymmetric imaginary part of σ_{bc}^{a,s^i} correspond to the conductivity under LPL and CPL, respectively. Note that Eq. (2) uses the velocity gauge, while the well-known shift and injection charge current formulae³⁵ use the length gauge. These two gauges are equivalent^{36,37} (Supplementary Information). An advantage of the velocity gauge is that the equations are relatively short and neat, and are easily generalizable to other responses under light, such as valley currents, static magnetization, etc.

The physical mechanism of BSPV can be better understood when compared with BPV. In Eq. (2), j^{a,s^i} with $i \neq 0$ is the spin current operator, defined as³⁸ $j^{a,s^i} = \frac{1}{2} (v^a s^i + s^i v^a)$. Here $s^i = \frac{\hbar}{2} \sigma^i$ is the spin operator with σ as the Pauli matrices. Note that there are lots of debates on the definition of spin current^{39–41}, see Supplementary Information for detailed discussions. If we define

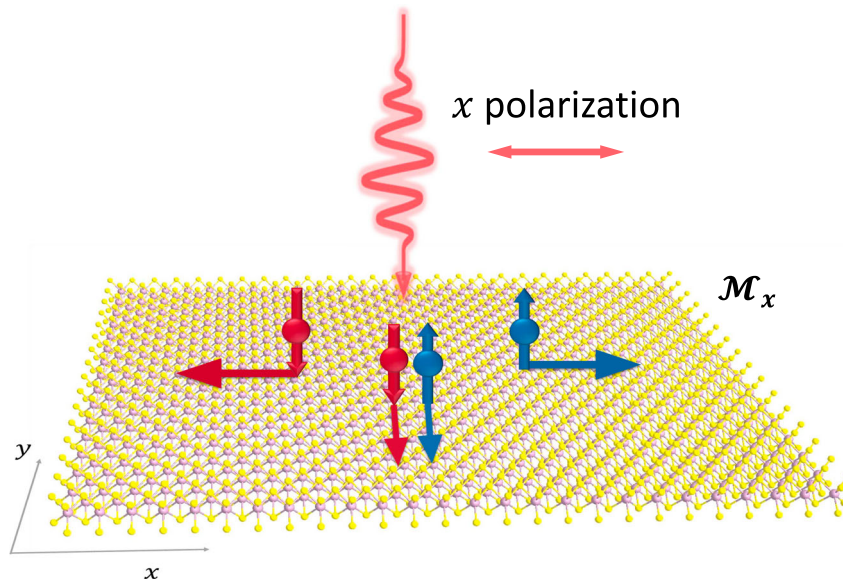


Fig. 1 A schematic illustration of pure spin and charge current. The light polarizes in the x-direction, while the system has mirror symmetry \mathcal{M}_x . In the x-direction, spin-up and spin-down states travel in opposite directions, so that the net charge current is vanishing, whereas the net spin current goes to the +x-direction. In the y-direction, spin-up and spin-down electrons travel in the same direction, leading to nonvanishing charge current but vanishing spin current.

$s^0 = e$, then j^{a,s^0} would indicate the charge current in BPV. The unified formula for spin and charge currents indicates that the DC spin current has a similar physical picture as the BPV, except that spin is a pseudovector; thus, it has different symmetries and selection rules from the charge, which is a scalar. When electron moves, its charge and spin would move simultaneously, leading to the charge and spin current, respectively. However, unlike charge, which is always $-|e|$ for an electron, spin does not necessarily have a specified value. A free electron can have equal probability to have $s_z = \frac{1}{2}$ or $-\frac{1}{2}$. When free electrons move to the right, the spin-z current associated would have an equal probability to be in the right (when $s_z = \frac{1}{2}$) or the left (when $s_z = -\frac{1}{2}$) direction, and the net spin current is thus zero⁴². Therefore, BSPV requires that the electrons have specified spin polarizations (i.e., a spin texture), which can be created by either spin-orbit coupling (SOC), or intrinsic magnetic ordering. Different from the formalism used in ref. 21, Eq. (2) does not require the spin to be a good quantum number or treat spin-up and spin-down states separately, so it can deal with arbitrary spin polarization under SOC. Later, we will show that treating SOC in such a rigorous way is of importance.

Next, we consider symmetry constraints on the conductivity tensor. First, the numerators in Eq. (2) are composed of terms with the format $N_{mnl}^{iabc} = j_{mn}^{a,s^i} v_{nl}^b v_{lm}^c$ ($i \neq 0$) for spin current and $N_{mnl}^{0abc} = v_{mn}^a v_{nl}^b v_{lm}^c$ ($i = 0$) for charge current. Under spatial inversion operation \mathcal{P} , one has $\mathcal{P}v_{mn}^a(\mathbf{k}) = -v_{mn}^a(-\mathbf{k})$, $\mathcal{P}s_{mn}^i(\mathbf{k}) = s_{mn}^i(-\mathbf{k})$, and $\mathcal{P}j_{mn}^{a,s^i}(\mathbf{k}) = -j_{mn}^{a,s^i}(\mathbf{k})$. Thus, $\mathcal{P}N_{mnl}^{iabc}(\mathbf{k}) = -N_{mnl}^{iabc}(-\mathbf{k})$ for both $i \neq 0$ and $i = 0$. On the other hand, the denominators in Eq. (2) are invariant under \mathcal{P} ; thus, all components (including charge and spin) of σ_{bc}^{a,s^i} should vanish after a summation over $\pm\mathbf{k}$ in \mathcal{P} -conserved systems. Therefore, the inversion symmetry \mathcal{P} has to be broken for both BPV and BSPV. Regarding time-reversal operation \mathcal{T} , one has $\mathcal{T}v_{mn}^a(\mathbf{k}) = -v_{mn}^{a*}(-\mathbf{k})$ and $\mathcal{T}s_{mn}^i(\mathbf{k}) = -s_{mn}^{i*}(-\mathbf{k})$ ($i \neq 0$). Here \bullet^* indicates complex conjugate of quantity \bullet . For charge current, one has $\mathcal{T}N_{mnl}^{0abc}(\mathbf{k}) = -N_{mnl}^{0abc*}(-\mathbf{k})$. Thus, the real and imaginary part of

N_{mnl}^{0abc} are odd and even under \mathcal{T} , respectively. The imaginary part of $N_{mnl}^{0abc}(\mathbf{k})$ contributes to the total charge conductivity after the summation over $\pm\mathbf{k}$ in a \mathcal{T} -conserved system. Similarly, for spin- i current ($i \neq 0$), one has $\mathcal{T}N_{mnl}^{iabc}(\mathbf{k}) = N_{mnl}^{iabc*}(-\mathbf{k})$; thus, it is the real part of $N_{mnl}^{iabc}(\mathbf{k})$ that contributes to the total spin conductivity. For both charge and spin current, \mathcal{T} does not need to be broken. Generally speaking, spin and charge currents should be generated simultaneously in the absence of \mathcal{P} . However, as we will show in detail later, a pure spin current can be realized if the system possesses mirror symmetry \mathcal{M}^d , inversion-mirror symmetry $\mathcal{P}\mathcal{M}^d$ or inversion-spin rotation symmetry $\mathcal{P}\mathcal{S}$. The behavior of relevant physical quantities under different symmetry operations is summarized in Table 1.

The carrier lifetime τ plays a rather important role. Here we use the charge current as the example; a similar analysis applies to the spin current. The DC photocurrent is basically $j^a = \sigma_{bc}^a E^b E^c$. If the system is nonmagnetic, and we use LPL, then it seems that \mathcal{T} should be preserved. In this case, seemingly σ_{bc}^a should be zero, because the j^a is odd under \mathcal{T} , while $E^b E^c$ is even. However, in practice the nonlinear photocurrent does exist, which is the BPV (shift current). In fact, here \mathcal{T} is effectively broken by dissipation in the thermodynamic second-law sense, characterized by τ . This is related to the well-known paradox regarding microscopic reversibility: if particles in a movie satisfy Newton's equations of motion, then its rewinding version ($t \rightarrow -t$) would also; thus, the apparent time-reversal symmetry in the equation of motion. However, if one watches the two movies ($t \rightarrow +t$ and $t \rightarrow -t$) for long enough time, then the "real" movie is the one with an overall "neater arrangement" of particles at the beginning of play, due to asymmetry in the initial condition. In other words, entropy creation indicates the "arrow of time" and distinguishes between t and $-t$. Therefore, it has been rationalized that the electronic relaxation time τ is indispensable for the shift current, although the shift-current conductivity σ_{bc}^a is (approximately) independent of τ ³⁵.

Dissipation occurs by the scattering of electrons and holes with phonons, etc., which lead to electron-hole recombination. The

Table 1 The behavior of physical quantities under symmetry operations.

	$v_{mn}^a(\mathbf{k})$	$s^i(\mathbf{k})$ ($i \neq 0$)	$N_{mnl}^{0abc}(\mathbf{k})$	$N^{iabc}(\mathbf{k})$ ($i \neq 0$)
\mathcal{P}	$-v_{mn}^a(-\mathbf{k})$	$s_{mn}^i(-\mathbf{k})$	$-N_{mnl}^{0abc}(-\mathbf{k})$	$-N_{mnl}^{iabc}(-\mathbf{k})$
\mathcal{T}	$-v_{mn}^{a*}(-\mathbf{k})$	$-s_{mn}^{i*}(-\mathbf{k})$	$-N_{mnl}^{0abc*}(-\mathbf{k})$	$N_{mnl}^{iabc*}(-\mathbf{k})$
\mathcal{PT}	$\tilde{v}_{mn}^a(\mathbf{k})$	$-\tilde{s}_{mn}^i(\mathbf{k})$	$\tilde{N}_{mnl}^{0abc*}(\mathbf{k})$	$-\tilde{N}_{mnl}^{iabc*}(\mathbf{k})$
\mathcal{M}^d	$(-1)^{\delta_{da}} v_{mn}^a(\mathbf{k}')$	$(-1)^{\delta_{di}} s_{mn}^i(\mathbf{k}')$	$[d; abc] \times N_{mnl}^{0abc}(\mathbf{k}')$	$(-1)^{\delta_{di}} [d; abc] \times N_{mnl}^{iabc}(\mathbf{k}')$
\mathcal{PM}^d	$(-1)^{\delta_{da}} v_{mn}^a(-\mathbf{k}')$	$(-1)^{\delta_{di}} s_{mn}^i(-\mathbf{k}')$	$-[d; abc] \times N_{mnl}^{0abc}(-\mathbf{k}')$	$(-1)^{\delta_{di}} [d; abc] \times N_{mnl}^{iabc}(-\mathbf{k}')$

Here $\tilde{\cdot}$ indicates \cdot obtained on the \mathcal{PT} partner state, which is degenerate in energy with the original state. $[d; abc]$ is -1 and $+1$ if there are odd and even numbers of d within a, b , and c . For example, $[x; xxx] = -1$, while $[x; xxy] = 1$. $\mathbf{k}' = \mathcal{M}^d \mathbf{k}$ is the mirror image of \mathbf{k} (only the d th component of \mathbf{k} is flipped).

scattering time τ is usually on the order of (sub)-picoseconds. In some cases, the spin relaxation time is short, then it can be a source of dissipation as well. Also, in the presence of scattering potentials (from e.g., impurities), there could be skew scattering^{43,44} and side jump^{45,46}, which lead to extrinsic spin/charge currents, as compared with the intrinsic currents studied in this work, that originates from the intrinsic band structure of the perfect crystal. Here we adopt the constant relaxation time approximation and use a constant $\tau = 0.2$ ps for all modes (band index n and wavevector k). In reality τ should be mode dependent (see Supplementary Information for more discussions) of course. This however does not affect the qualitative features of the theory.

To illustrate the theory, we investigate three distinct material systems: (1) monolayer transition metal dichalcogenides (TMD), which are \mathcal{P} -broken but \mathcal{T} -preserved; (2) antiferromagnetic bilayers MnBi_2Te_4 (MBT), which is \mathcal{P} - and \mathcal{T} -broken but \mathcal{PT} -preserving; (3) the $\{001\}$ surface of cubic SnTe , which is \mathcal{P} -broken, but has double mirror symmetry \mathcal{M}_x and \mathcal{M}_y . The results suggest that BSPV is generic and robust in these distinct systems. We only show the NLO charge and spin current under LPL, while the responses under CPL can be found in the Supplementary Information.

Monolayer TMD. 2H-phase TMDs are well-studied 2D materials that possess many exotic electronic and optical properties. We take monolayer 2H MoS_2 as an example. The atomic structure of monolayer 2H MoS_2 (space group $P6m2$) is shown in the inset of Fig. 2e, which lacks \mathcal{P} , but is invariant under \mathcal{M}^x and \mathcal{M}^z . Monolayer TMDs exhibit Zeeman-type (out-of-plane) spin splitting due to the in-plane anisotropy. This could be understood with the effective magnetic field from SOC, expressed as $\mathbf{B}_{\text{eff}} = \frac{1}{2m_e c^2} \mathbf{p} \times \nabla V$, where m_e is the electron mass and c is the speed of light. In monolayer TMDs, the momentum \mathbf{p} is in the in-plane (x - y) direction, while ∇V is also largely in the x - y plane, due to the mirror plane \mathcal{M}^z . As a result, \mathbf{B}_{eff} is mainly along the out-of-plane direction, leading to the Zeeman-type spin splitting. These arguments are verified by the spin texture $s_{mn}^i(\mathbf{k}) = \langle m\mathbf{k} | \sigma_i | m\mathbf{k} \rangle$ from ab initio calculations. Figure 2a, b show $s_{mn}^z(\mathbf{k})$ for the highest valence band and the lowest conduction band of MoS_2 , respectively. One can see that $s_{mn}^z(\mathbf{k}) \cong \pm 1$ for nearly all \mathbf{k} -points. Also, $s_{mn}^z(\mathbf{k})$ is opposite near the K and K' valleys, which is the spin-valley locking^{47,48}.

Here we need to examine constraints on NLO spin or charge current from mirror symmetry \mathcal{M}^d (Table 1). The polar vector v_{mn}^a satisfies $\mathcal{M}^d v_{mn}^a(\mathbf{k}) = (-1)^{\delta_{da}} v_{mn}^a(\mathbf{k}')$, where \mathbf{k}' is the image of \mathbf{k} under \mathcal{M}^d (only the d -th component flips its sign), whereas the axial vector s_{mn}^i should satisfy $\mathcal{M}^d s_{mn}^i(\mathbf{k}) = -(-1)^{\delta_{di}} s_{mn}^i(\mathbf{k}')$. Therefore, one has $\mathcal{M}^d N_{mnl}^{0abc}(\mathbf{k}) = -N_{mnl}^{0abc}(\mathbf{k}')$ when there are odd number of d within a, b , and c , and the charge current should

vanish in this case. For example, when the system has \mathcal{M}^x , then σ_{xx}^{x,s^0} and σ_{yy}^{x,s^0} should vanish. On the other hand, if $d \neq i$, the spin- i current should vanish when there are even number of d within a, b , and c , because the \mathcal{M}^d operation on s^i contributes to an additional sign change if $d \neq i$. Therefore, σ_{xx}^{x,s^z} and σ_{yy}^{x,s^z} could exist in the presence of \mathcal{M}^x . Due to the opposite behavior of N_{mnl}^{0abc} and N_{mnl}^{iabc} under \mathcal{M}^d , a pure spin current can be generated.

The calculated NLO spin and charge conductivity of monolayer MoS_2 under different light polarizations are shown in Fig. 2e, f. One can see that with in-plane polarized light, the nonzero conductivities are complementary for spin and charge currents, consistent with the analysis above. In detail, under the x -polarized light, the charge current is along y -direction ($\sigma_{xx}^{x,s^0} = 0$ and $\sigma_{xx}^{y,s^0} \neq 0$), whereas the spin- z current is along the x -direction ($\sigma_{xx}^{x,s^z} \neq 0$ and $\sigma_{xx}^{y,s^z} = 0$). This indicates that along x -direction, equal numbers of spin-up and spin-down electrons are moving oppositely, so the net charge flux is zero, while the net spin flux is nonzero. Along y -direction, the spin-up and spin-down carriers move in the same direction, leading to zero spin current but nonzero charge current (Fig. 1). Similar effects occur as well in the case of y -polarized light. Interestingly, the spin- z conductivity can be larger than the charge conductivity (in the sense of equivalating $\frac{\hbar}{2} = |e|$). This should be compared with the linear spin Hall effect, where the spin Hall angle (the ratio between the spin conductivity to charge conductivity) is usually on the order of 0.1 and below⁴⁹. We also plot the \mathbf{k} -specific contribution to the total conductivity, defined as $I_{bc}^{a,s^i}(\omega, \mathbf{k}) = \text{Re} \left\{ \sum_{mnl} \frac{f_{lm}^a v_{lm}^b}{E_{ml} - \hbar\omega + i\delta} \left(\frac{v_{mn}^{a,s^i} v_{nl}^c}{E_{mn} + i\delta} - \frac{v_{ml}^{a,s^i} v_{nl}^c}{E_{nl} + i\delta} \right) \right\}$, in Fig. 2c, d for σ_{xx}^{x,s^z} and σ_{yy}^{y,s^0} at $\omega = 2.8$ eV. The mirror symmetry $k_x \rightarrow -k_x$ can be clearly observed.

As discussed before, the generation of spin current requires a spin texture. For MoS_2 , the spin texture is generated by SOC. When SOC is turned off, the spins of electrons are unpolarized, and the spin current would be zero. This is verified by our ab initio calculations. We artificially rescale the strength of SOC in MoS_2 by a factor of λ , and $\lambda = 0$ ($\lambda = 1$) corresponds to no (full) SOC. The NLO conductivities as a function of λ are shown in Fig. 2g, h. One can see that when $\lambda = 0$, the spin conductivity is indeed zero. As λ increases, the spins would have more and more specified polarization, and the spin conductivity increase accordingly. In contrast, the charge conductivity is nearly independent of λ .

Bilayer antiferromagnetic MBT. Next, we study the bilayer AFM MBT^{50,51}, where a large NLO charge current has been reported^{52,53}. Each layer of MBT is a septuple layer (SL) in the sequence of Te-Bi-Te-Mn-Te-Bi-Te. The Mn atoms possess

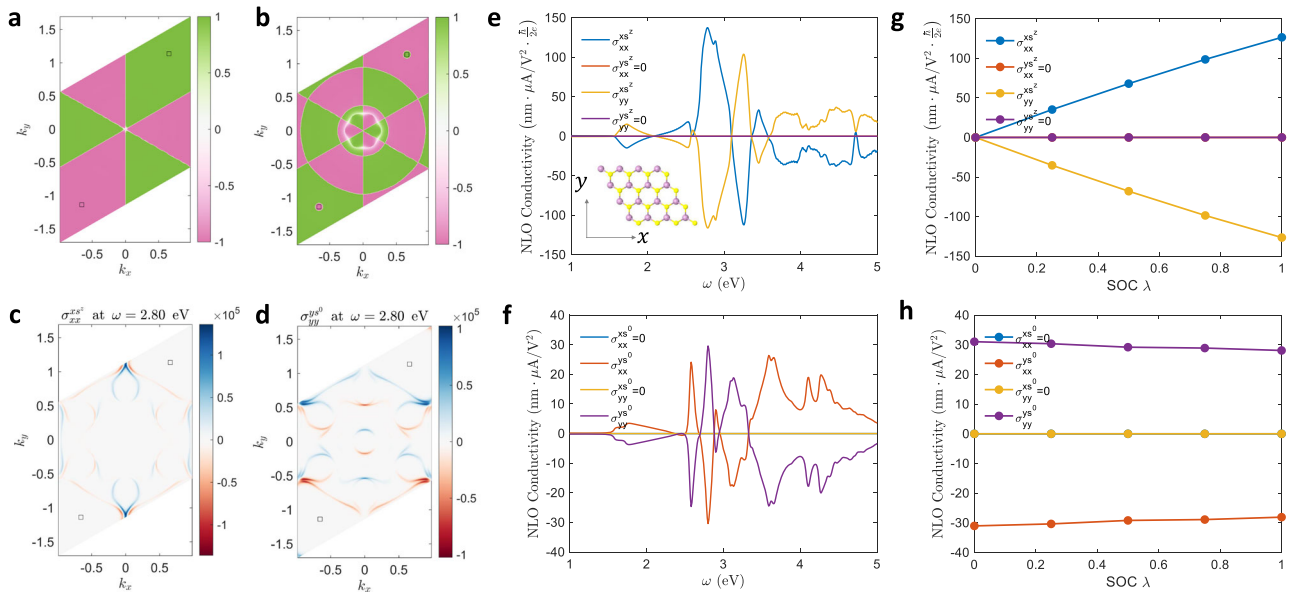


Fig. 2 NLO spin current of MoS₂. **a, b** The spin-z texture $S_{mm}^z(\mathbf{k})$ for the **a** highest valence band and **b** lowest conduction band of MoS₂. Nearly all k -points have $S_{mm}^z(\mathbf{k}) \cong \pm 1$. **(c, d)** k -specified contribution to the total photoconductivity $\sigma_{xx}^{xs^z}$ and $\sigma_{yy}^{ys^z}$. The black boxes in **(a-d)** indicate K and K' points in the BZ. **e, f** The NLO spin-z and charge conductivity. The complementary behavior is clearly observable: the spin and charge currents are in perpendicular directions. Inset of **(e)**: the atomic structure of MoS₂. **g, h** Peak values of NLO spin **(g)** and charge **(h)** conductivity of MoS₂ as a function of SOC strength λ . The spin conductivity grows linearly with SOC strength, while the charge conductivity is almost independent of SOC strength.

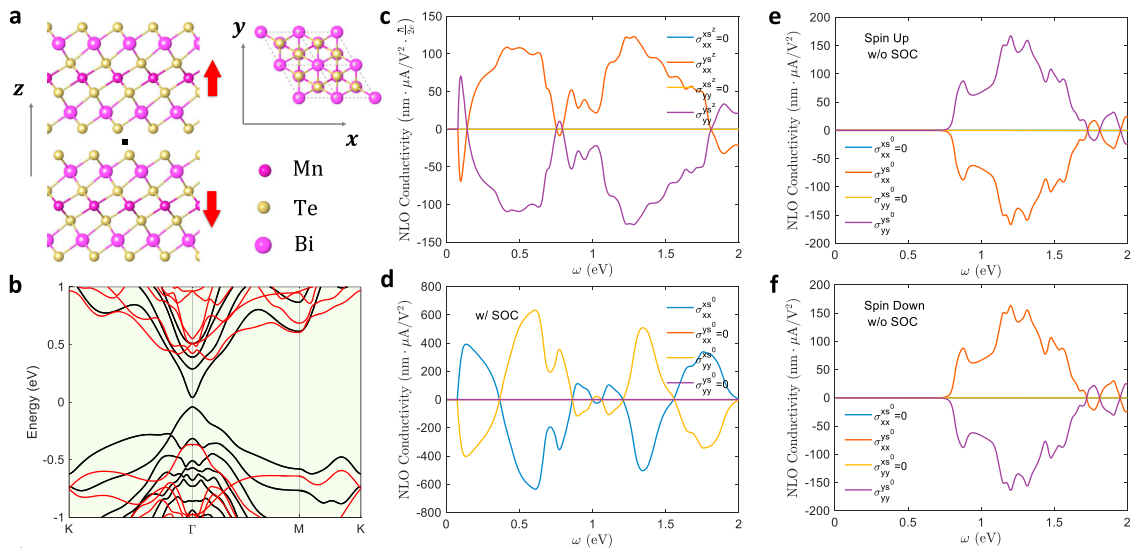


Fig. 3 NLO spin current of MBT. **a** Atomic structure of bilayer MnBi₂Te₄. The atomic structure has both inversion symmetry \mathcal{P} and mirror symmetry \mathcal{M}^x . The inversion center is in between the two layers (black square). The magnetic momentum on Mn is indicated by the red arrows. Considering magnetism, both \mathcal{P} and \mathcal{M}^x break. **b** Band structure of MBT with (black) and without (red) SOC. **c, d** The NLO spin and charge photoconductivity of bilayer MnBi₂Te₄ with SOC. Both spin and charge currents have nonzero components and exhibit complementary behavior. **e, f** The NLO charge conductivity without SOC. The spin-up and spin-down states are treated separately. The photoconductivity from spin-up and spin-down states are exactly opposite to each other. Therefore, the total charge conductivity is zero. But the spin-z conductivity is nonzero.

magnetic moments $\sim 5\mu_B$, with intra-plane ferromagnetic ordering. Bulk MBT is composed of van der Waals (vdW) stacked SLs with inter-plane AFM ordering, and the AFM nature persists when MBT is thinned down to multiple atomic layers. In particular, bilayer MBT is a compensated AFM insulator, whose atomic structure is shown in Fig. 3a. The ground state magnetic moments are pointing along the z -direction with a magnetic point group of $\bar{3}'m'$. The atomic

structure of bilayer MBT is invariant under \mathcal{P} and the inversion center lies in the vdW gap between the two layers (black square in Fig. 3a). However, when one considers magnetism, both \mathcal{P} and \mathcal{T} are broken. Nevertheless, AFM bilayer MBT is invariant under the combined operation \mathcal{PT} . Similarly, we find that $\mathcal{PM}^d_{mn}(\mathbf{k}) = -(-1)^{\delta_{ab}} \nu_{mn}^a(-\mathbf{k})$ and $\mathcal{PM}^d_{mn}(\mathbf{k}) = -(-1)^{\delta_{di}} s_{mn}^i(-\mathbf{k})$. Then, one can see that when

$d \neq i$, N^{0abc} (N^{iabc}) should vanish after Brillouin zone integration when there are even (odd) number of d within a, b , and c . Therefore, one can still obtain a pure spin current in systems with \mathcal{PM}^d due to the different selection rule on charge and spin currents.

The band structures of bilayer MBT with and without SOC are shown in Fig. 3b. The bandgap is ~ 0.1 eV and is located at the Γ point when the SOC effect is included, whereas it is ~ 0.7 eV and is indirect without SOC. As shown in Fig. 3c–f, the SOC also makes a significant difference in the NLO spin and charge conductivity. When SOC is turned off, s^z is a good quantum number. States with $s^z = \pm 1$ are strictly degenerate in an AFM system and can be treated separately. The NLO conductivities without SOC are shown in Fig. 3e, f, where one can see that the charge current from spin-up (j_{\uparrow}) and spin-down (j_{\downarrow}) states are exactly opposite to each other. Consequently, the total charge current $j^0 = j_{\uparrow} + j_{\downarrow}$ is zero. However, the total spin- z current $j^{sz} = j_{\uparrow} - j_{\downarrow}$ is nonzero. Therefore, a pure spin current without any charge current is predicted, which comes from the inversion-spin rotation symmetry \mathcal{PS} . These results are consistent with those in ref. 19, where several other well-known AFM materials such as NiO and BiFeO₃ were studied.

However, SOC would break \mathcal{PS} , and thus lead to a nonzero charge current. Due to the \mathcal{PM}^x symmetry, the charge current is perpendicular to the spin- z current (Fig. 3c, d). We also artificially rescale the strength of SOC by a factor of λ , as done in the MoS₂ section (see Supplementary Information). It is found that the charge conductivity increases with λ . This is because with a larger λ , the spin and orbital degrees of freedom are coupled more strongly, and inversion-spin rotation symmetry \mathcal{PS} is broken to a greater extent; thus, the charge conductivity would be larger. These results suggest that while SOC enables spin current in nonmagnetic materials such as MoS₂, it would adversely hinder the generation of pure spin current in some cases. Also, SOC should be treated rigorously when studying both the spin current and the charge current.

2D surface of 3D topological materials. Topological insulators^{54–56} (TIs) and topological semimetals^{57,58} have attracted intense interest in recent years. In TIs, the bulk states are insulating with a finite bandgap, while the surface states are (semi)-metallic with symmetry-protected vanishing bandgap, which has potential applications in electronic and spintronic devices. One salient feature of the surface states is the spin-momentum locking, which could prevent the electrons from backscattering and facilitate spin manipulations^{59–61}. In addition, the inversion symmetry \mathcal{P} is naturally broken on the surfaces, even if the bulk possesses \mathcal{P} . Therefore, the NLO charge⁶² and spin current can be induced solely on surfaces, while the bulk remains silent.

Here we take the topological crystalline insulator (TCI)^{63,64} cubic SnTe as an example. The bulk SnTe has space group $Fm\bar{3}m$, and is inversion symmetric inside the 3D crystal, which forbids BPV/BSPV in the bulk interior. But the 2D surfaces of this 3D crystal would lose the inversion symmetry, and therefore can support both BPV and BSPV. Here we consider the $\{001\}$ surface, which has a four-fold rotational symmetry and double mirror symmetries \mathcal{M}^x and \mathcal{M}^y (Fig. 4a). The spectrum function $A(\mathbf{k}, \omega)$ of the $\{001\}$ surface is obtained with iterative Green's function method^{65,66} and is shown in Fig. 4b, c. In Fig. 4b, $A(\mathbf{k}, \omega)$ along high-symmetry lines in the BZ is presented, and the gapless surface states can be clearly observed. In Fig. 4c, $A(\mathbf{k}, \omega)$ near \bar{X} point in the BZ with selected energy $\omega = -0.2, 0$, and 0.2 eV are plotted. One can see that $A(\mathbf{k}, \omega)$ can have significant

values on the same \mathbf{k} -point with different ω , enabling strong interband transitions and significant photocurrents. In addition, the surface spin textures are plotted as black arrows. The nonzero s^x and s^y components indicate that one can obtain spin- x and spin- y currents.

According to our previous symmetry analysis, under in-plane polarized light ($b, c = x$ or y), no NLO charge or spin- z current can be generated on the $\{001\}$ surface, due to the double mirror symmetry \mathcal{M}_x and \mathcal{M}_y . However, it is possible to have nonzero spin- x and spin- y currents, which is verified by our ab initio calculations. We use a slab model to compute the surface NLO spin and charge conductivity. To distinguish the contribution from only one surface of the slab, we define a projection operator⁶⁷ $P_l = \sum_{i \in l} |\psi_i\rangle \langle \psi_i|$. Here $|\psi_i\rangle$ are atomic orbitals centered on the l -th atomic layer. Then, we replace the current operator j in Eq. (2) with $P_l j P_l$, and the resultant conductivity can be layer distinguished (on the l th layer). Note that there could be nonzero cross-terms $P_l j P_m$ (with $l \neq m$), indicating the interference between the l th and m th layer. From our computations, even for neighboring layers with $m = l \pm 1$, the contribution from $P_l j P_m$ is quite small ($< 10\%$). Here for a conceptual demonstration of our theory, we only consider $P_{l=1} j P_{l=1}$ and calculate the contribution from the out-most layer. NLO spin- x and spin- y conductivities are plotted in Fig. 4d. One can see that the maximum value of $\sigma_{yy}^{ys^x}$ can reach $500 \text{ nm} \times \mu\text{V}/\text{A}^2 \times \frac{\hbar}{2e}$. We would like to emphasize again that under the light field with in-plane polarization, NLO charge current is absent on this $\{001\}$ surface; therefore, a pure spin current without any charge current can be generated due to the double mirror symmetries. Such methodology can also be used to distinguish surface and bulk states and to probe the surface states. There may be other systems that possess double mirror symmetries as well, such as monolayer FeSe⁶⁸, which may be good candidates for pure spin current generation.

Discussions

Before concluding, we would like to make some remarks. First, it is well known that BPV has potentially shift and injection current contributions. The shift mechanism comes from the fact that the wavefunction center of the electron and hole band states are different, leading to an electric dipole upon photon absorption. On the other hand, the injection mechanism comes from the fact that the electron and holes have different velocities, and that the coherent \mathbf{k} and $-\mathbf{k}$ excitations are imbalanced, leading to \mathbf{k} and $-\mathbf{k}$ asymmetry in steady-state population and a net current. These facts are more evident if we transform Eq. (2) into the length gauge, as shown in Supplementary Information. In a \mathcal{T} -conserved system, the DC charge currents under LPL and CPL have shift and injection mechanism, respectively³⁵. In contrast, for the DC spin current, the mechanism under LPL and CPL should be injection-like and (shift + injection)-like (see Supplementary information). Here the shift- (injection-) current is defined by the conductivity scaling relationship as $\propto \tau^0$ (τ^1). Therefore, the spin conductivity in Figs. 2e and 4d can be further enhanced if a larger τ is used (see Supplementary Information). The different mechanisms for spin and charge current come from the different behavior of N_{mnl}^{iabc} ($i \neq 0$) and N_{mnl}^{0abc} under \mathcal{T} -operation. Note that in \mathcal{T} -conserved systems, the shift spin current should vanish under LPL, consistent with the arguments in ref. 20. We have done similar analyses on mechanisms of current generation under different symmetry conditions, and the results are listed in Table 2. These results are also computationally verified by varying τ (see details in Supplementary Information).

Second, as shown above, a pure spin current induced by mirror symmetry is usually accompanied by a charge current in the transverse direction (except for the $\{100\}$ surface states of cubic

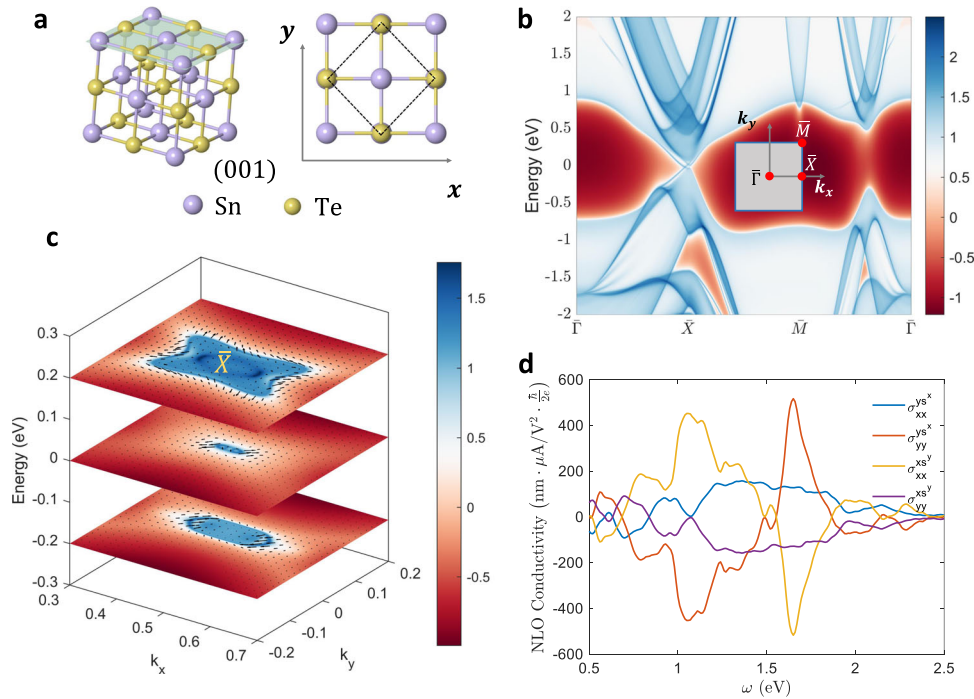


Fig. 4 NLO spin current on the (001) surface of SnTe. **a** The atomic structure of SnTe. In the left panel the {001} face is painted in light green, which possesses double mirror symmetries \mathcal{M}^x and \mathcal{M}^y . The dashed box in the right panel indicates the primitive cell on the surface. **b** The surface spectrum function $A(\mathbf{k}, \omega)$ on high-symmetry lines in the BZ. The gapless surface states can be observed. **c** The surface spectrum function $A(\mathbf{k}, \omega)$ over the BZ for selected $\omega = -0.2, 0,$ and 0.2 eV. k_x and k_y are in the unit of reciprocal lattices. The surface spin textures are indicated by the black arrows. Color scheme (red to blue) in **(b, c)** represents surface state contribution. The color bars are in logarithmic scale, and the energy is offset to the valence band maximum. **d** The NLO spin current conductivity with x and y spin polarizations. Note that all charge and spin-z current components are vanishing due to \mathcal{M}^x and \mathcal{M}^y .

Table 2 Mechanisms for NLO charge and spin current generation under different material symmetries and light polarizations.

	\mathcal{P} -conserved	\mathcal{P} -broken, \mathcal{T} -conserved	\mathcal{P} -broken, \mathcal{T} -broken \mathcal{PT} -conserved	\mathcal{P} -broken, \mathcal{T} -broken \mathcal{PT} -broken
DC charge current (BPV)	No	LPL \iff shift CPL \iff injection	LPL \iff injection CPL \iff shift + injection	LPL \iff shift + injection CPL \iff shift + injection
DC spin current (BSPV)	No	LPL \iff injection CPL \iff shift + injection	LPL \iff shift CPL \iff injection	LPL \iff shift + injection CPL \iff shift + injection

For the shift mechanism, the conductivity contribution is independent of the carrier lifetime τ . For the injection mechanism, the conductivity contribution scales linearly with τ .

SnSe, with double mirror symmetry \mathcal{M}^x and \mathcal{M}^y). It is possible to achieve a pure spin current without any charge current at all, if the system possesses inversion-spin rotation symmetry \mathcal{PS} . One can see that $\mathcal{PSN}_{mnl}^{0abc}(\mathbf{k}) = -\hat{N}_{mnl}^{0abc}(-\mathbf{k})$, where $\hat{\cdot}$ indicates \cdot obtained on the spin partner state. Therefore, the charge current should identically be zero in the presence of \mathcal{PS} . On the other hand, $\mathcal{PSN}_{mnl}^{iabc}(\mathbf{k}) = -e^{i\phi} \hat{N}_{mnl}^{iabc}(-\mathbf{k})$, where $e^{i\phi}$ is a phase factor induced by the spin rotation operation on s^i . Thus, the spin current does not have to vanish. In fact, \mathcal{PS}_z , where S_z flips the spin-up and spin-down states, is the origin of the vanishing charge current of MBT when SOC is ignored. In practice, a skyrmion lattice, or magnetic materials with canted or all-in-all-out magnetic ordering, can be an ideal platform for the generation of pure spin current without any charge current.

Third, the NLO conductivity in Eq. (2) is obtained from the quadratic response theory. It essentially is $\text{Tr}(j^{(0)}\rho^{(2)})$, where $j^{(0)}$ is the current operator independent of the electric field E , while $\rho^{(2)}$ is the second-order perturbation in the density matrix and is

proportional to E^2 . There could be other mechanisms for the generation of spin/charge current. For example, there could be an anomalous velocity, which leads to an additional term $j^{(1)}$ in the current operator that is linearly dependent on E . $j^{(1)}$ can contribute to an NLO conductivity from $\text{Tr}(j^{(1)}\rho^{(1)})$, where $\rho^{(1)}$ is the first-order perturbation in the density matrix. Note that this contribution should vanish for all the material systems studied in this work.

Finally, we would like to briefly discuss how the spin current can be detected. There are well-established approaches for detecting the spin current generated by, e.g., spin Hall effect⁹. For example, with an open-circuit setup (Supplementary Information and Figure S2a), the spin would accumulate on the ends of the source material. The spin accumulation can be measured by magneto-optic effects such as Kerr rotation or Faraday effect⁶⁹. Also, in a close circuit setup (Supplementary Information and Figure S2b), the spin current source is sandwiched between two metallic leads (e.g., Pt). The light-induced spin current is

transmitted to the metallic leads. An inverse spin Hall voltage would be generated transverse to the spin current^{70–72}, and the spin current can be measured by the inverse spin Hall voltage. Assuming a spin conductivity of $100 \mu\text{A}/\text{V}^2 \frac{\hbar}{2e}$, an electric field as small as $100 \text{ V}/\text{m}$ would generate a spin current density of $1 \text{ A}/\text{m}^2 \frac{\hbar}{2e}$. Assume a spin Hall angle of 0.1, the current density in the metallic lead would be $10 \text{ A}/\text{m}^2$, which can be detectable.

In conclusion, we demonstrate a generic picture of spin photocurrent generation with nonlinear light–matter interactions. By symmetry analysis, we reveal that this effect does not have any special requirements, except for the inversion symmetry breaking. Thus, it applies to a wide range of materials and extended defects like surfaces, stacking faults, grain boundaries, and dislocations. If the system possesses mirror symmetry or inversion-mirror symmetry, a pure spin current can be realized. Our theory is verified with ab initio calculations in several material systems, and the spin current conductivity is found to be comparable or even bigger than its charge BPV cousin. The predicted BSPV platforms can be readily integrated with existing semiconductor technologies. They may find applications in next-generation ultrafast spintronics and quantum information processing.

Methods

The first-principles calculations are based on density functional theory (DFT)^{73,74} as implemented in the Vienna ab initio simulation package^{75,76}. The exchange–correlation interactions are treated by a generalized gradient approximation in the form of Perdew–Burke–Ernzerhof⁷⁷. Core and valence electrons are treated by projector augmented wave method⁷⁸ and plane-wave basis functions, respectively. For DFT calculations, the first Brillouin zone is sampled by a Γ -centered k -mesh with grid density of at least $2\pi \times 0.02 \text{ \AA}^{-1}$ along each dimension. The DFT + U method is adopted to treat the d orbitals of Mn atoms in MBT ($U = 4.0 \text{ eV}$). Then a tight-binding (TB) Hamiltonian is constructed from DFT results with the help of the Wannier90 package⁷⁹. The TB Hamiltonian is utilized to calculate the NLO charge and spin conductivity according to Eq. (2) on a finer k -mesh. The k -mesh convergence for BZ integration is well tested. In practice, the BZ integration in Eq. (2) is carried out by k -mesh sampling with $\int \frac{dk}{(2\pi)^3} = \frac{1}{V} \sum_k w_k$, where V is the volume of the simulation cell in real space and w_k is weight factor. However, for 2D materials, the definition of volume V is ambiguous, because the thickness of 2D materials is ambiguously defined⁸⁰. Thus, we replace volume V with the area S , and the 2D and 3D conductivity satisfy $\sigma_{2D} = L\sigma_{3D}$, where L is an effective thickness of the material.

Data availability

The authors declare that the main data supporting the findings of this study are available within the article and its Supplementary information files.

Code availability

The MATLAB code for computing the NLO conductivities is available from the corresponding author upon reasonable request.

Received: 21 December 2020; Accepted: 16 June 2021;

Published online: 15 July 2021

References

- Žutić, I., Fabian, J. & Sarma, S. Das Spintronics: fundamentals and applications. *Rev. Mod. Phys.* **76**, 323–410 (2004).
- Bader, S. D. & Parkin, S. S. P. Spintronics. *Annu. Rev. Condens. Matter Phys.* **1**, 71–88 (2010).
- Shor, P. W. *Algorithms for Quantum Computation: Discrete Logarithms and Factoring*, 124–134 (Institute of Electrical and Electronics Engineers, 2002).
- Ladd, T. D. et al. Quantum computers. *Nature* **464**, 45–53 (2010).
- Umesh, S. & Mittal, S. A survey of spintronic architectures for processing-in-memory and neural networks. *J. Syst. Archit.* **97**, 349–372 (2019).
- Awschalom, D. D. & Flatté, M. E. Challenges for semiconductor spintronics. *Nat. Phys.* **3**, 153–159 (2007).
- Ganichev, S. D. et al. Spin-galvanic effect. *Nature* **417**, 153–156 (2002).
- Benítez, L. A. et al. Tunable room-temperature spin galvanic and spin Hall effects in van der Waals heterostructures. *Nat. Mater.* **19**, 170–175 (2020).
- Sinova, J., Valenzuela, S. O., Wunderlich, J., Back, C. H. & Jungwirth, T. Spin Hall effects. *Rev. Mod. Phys.* **87**, 1213–1260 (2015).
- D'Yakonov, M. I., Perel', V. I., D'Yakonov, M. I. & Perel', V. I. Possibility of orienting electron spins with current. *JETPL* **13**, 467 (1971).
- Dyakonov, M. I. & Perel, V. I. Current-induced spin orientation of electrons in semiconductors. *Phys. Lett. A* **35**, 459–460 (1971).
- Ando, K. et al. Inverse spin-Hall effect induced by spin pumping in metallic system. *J. Appl. Phys.* **109**, 103913 (2011).
- Uchida, K. et al. Observation of the spin Seebeck effect. *Nature* **455**, 778–781 (2008).
- Adachi, H., Uchida, K., Saitoh, E. & Maekawa, S. Theory of the spin Seebeck effect. *Rep. Prog. Phys.* **76**, 036501 (2013).
- Sheng, P. et al. The spin Nernst effect in tungsten. *Sci. Adv.* **3**, e1701503 (2017).
- Meyer, S. et al. Observation of the spin Nernst effect. *Nat. Mater.* **16**, 97–981 (2017).
- Ganichev, S. D. et al. Conversion of spin into directed electric current in quantum wells. *Phys. Rev. Lett.* **86**, 4358–4361 (2001).
- Luo, Y. K. et al. Opto-valleytronic spin injection in monolayer MoS₂/few-layer graphene hybrid spin valves. *Nano Lett.* **17**, 3877–3883 (2017).
- Young, S. M., Zheng, F. & Rappe, A. M. Prediction of a linear spin bulk photovoltaic effect in antiferromagnets. *Phys. Rev. Lett.* **110**, 057201 (2013).
- Kim, K. W., Morimoto, T. & Nagaosa, N. Shift charge and spin photocurrents in Dirac surface states of topological insulator. *Phys. Rev. B* **95**, 035134 (2017).
- Ishizuka, H. & Sato, M. Rectification of spin current in inversion-asymmetric magnets with linearly polarized electromagnetic waves. *Phys. Rev. Lett.* **122**, 197702 (2019).
- Ishizuka, H. & Sato, M. Theory for shift current of bosons: photogalvanic spin current in ferrimagnetic and antiferromagnetic insulators. *Phys. Rev. B* **100**, 224411 (2019).
- Žutić, I., Fabian, J. & Das Sarma, S. Proposal for a spin-polarized solar battery. *Appl. Phys. Lett.* **79**, 1558–1560 (2001).
- Žutić, I., Fabian, J., Fabian, J. & Das Sarma, S. Spin-polarized transport in inhomogeneous magnetic semiconductors: theory of magnetic/nonmagnetic p-n junctions. *Phys. Rev. Lett.* **88**, 66603/1–66603/4 (2002).
- Endres, B. et al. Demonstration of the spin solar cell and spin photodiode effect. *Nat. Commun.* **4**, 1–5 (2013).
- Stevens, M. J. et al. Quantum interference control of ballistic pure spin currents in semiconductors. *Phys. Rev. Lett.* **90**, 4 (2003).
- Hübner, J. et al. Direct observation of optically injected spin-polarized currents in semiconductors. *Phys. Rev. Lett.* **90**, 4 (2003).
- Hamamoto, K., Ezawa, M., Kim, K. W., Morimoto, T. & Nagaosa, N. Nonlinear spin current generation in noncentrosymmetric spin-orbit coupled systems. *Phys. Rev. B* **95**, 224430 (2017).
- Belinicher, V. I. & Sturman, B. I. The photogalvanic effect in media lacking a center of symmetry. *Sov. Phys. Usp.* **23**, 199–223 (1980).
- Von Baltz, R. & Kraut, W. Theory of the bulk photovoltaic effect in pure crystals. *Phys. Rev. B* **23**, 5590–5596 (1981).
- Fert, A. Nobel lecture: origin, development, and future of spintronics nobel lecture: origin, development, and future of spintronics. *Rev. Mod. Phys.* **80**, 1517–1530 (2008).
- Puebla, J., Kim, J., Kondou, K. & Otani, Y. Spintronic devices for energy-efficient data storage and energy harvesting. *Commun. Mater.* **1**, 1–9 (2020).
- Bernevig, B. A. & Zhang, S. C. Quantum spin hall effect. *Phys. Rev. Lett.* **96**, 106802 (2006).
- Kraut, W. & Baltz, R. Anomalous bulk photovoltaic effect in ferroelectrics: a quadratic response theory. *Phys. Rev. B* **19**, 1548–1554 (1979).
- Sipe, J. & Shkrebtii, A. Second-order optical response in semiconductors. *Phys. Rev. B* **61**, 5337–5352 (2000).
- Ventura, G. B., Passos, D. J., Lopes Dos Santos, J. M. B., Viana Parente Lopes, J. M. & Peres, N. M. R. Gauge covariances and nonlinear optical responses. *Phys. Rev. B* **96**, 035431 (2017).
- Taghizadeh, A., Hipolito, F. & Pedersen, T. G. Linear and nonlinear optical response of crystals using length and velocity gauges: effect of basis truncation. *Phys. Rev. B* **96**, 195413 (2017).
- Sinova, J. et al. Universal intrinsic spin Hall effect. *Phys. Rev. Lett.* **92**, 126603 (2004).
- Rashba, E. I. Spin currents in thermodynamic equilibrium: the challenge of discerning transport currents. *Phys. Rev. B* **68**, 241315 (2003).
- Shi, J., Zhang, P., Xiao, D. & Niu, Q. Proper definition of spin current in spin-orbit coupled systems. *Phys. Rev. Lett.* **96**, 076604 (2006).
- Sun, Q. F., Xie, X. C. & Wang, J. Persistent spin current in nanodevices and definition of the spin current. *Phys. Rev. B* **77**, 035327 (2008).
- Fei, R., Lu, X. & Yang, L. Intrinsic spin photogalvanic effect in nonmagnetic insulator. Preprint at [arXiv https://arxiv.org/abs/2006.10690](https://arxiv.org/abs/2006.10690) (2020).
- Smit, J. The spontaneous hall effect in ferromagnetics I. *Physica* **21**, 877–887 (1955).
- Smit, J. The spontaneous hall effect in ferromagnetics II. *Physica* **24**, 39–51 (1958).

45. Berger, L. Influence of spin-orbit interaction on the transport processes in ferromagnetic nickel alloys, in the presence of a degeneracy of the 3d band. *Physica* **30**, 1141–1159 (1964).
46. Berger, L. Side-jump mechanism for the hall effect of ferromagnets. *Phys. Rev. B* **2**, 4559–4566 (1970).
47. Zeng, H. et al. Optical signature of symmetry variations and spin-valley coupling in atomically thin tungsten dichalcogenides. *Sci. Rep.* **3**, 1–5 (2013).
48. Bawden, L. et al. Spin-valley locking in the normal state of a transition-metal dichalcogenide superconductor. *Nat. Commun.* **7**, 1–6 (2016).
49. Gradhand, M., Fedorov, D. V., Zahn, P. & Mertig, I. Spin Hall angle versus spin diffusion length: tailored by impurities. *Phys. Rev. B* **81**, 245109 (2010).
50. Li, J. et al. Intrinsic magnetic topological insulators in van der Waals layered MnBi_2Te_4 -family materials. *Sci. Adv.* **5**, eaaw5685 (2019).
51. Deng, Y. et al. Quantum anomalous Hall effect in intrinsic magnetic topological insulator MnBi_2Te_4 . *Science* **367**, 895–900 (2020).
52. Wang, H. & Qian, X. Giant nonlinear photocurrent in \mathbb{Z}_2 -symmetric magnetic topological quantum materials. *npj Comput. Mater.* **6**, 199 <https://doi.org/10.1038/s41524-020-00462-9> (2020).
53. Fei, R., Song, W. & Yang, L. Giant linearly-polarized photogalvanic effect and second harmonic generation in two-dimensional axion insulators. *Phys. Rev. B* **102**, 035440 (2020).
54. Hasan, M. Z. & Kane, C. L. Colloquium: topological insulators. *Rev. Mod. Phys.* **82**, 3045–3067 (2010).
55. Qi, X. L. & Zhang, S. C. Topological insulators and superconductors. *Rev. Mod. Phys.* **83**, 1057 (2011).
56. Bansil, A., Lin, H. & Das, T. Colloquium: topological band theory. *Rev. Mod. Phys.* **88**, 021004 (2016).
57. Armitage, N. P., Mele, E. J. & Vishwanath, A. Weyl and Dirac semimetals in three-dimensional solids. *Rev. Mod. Phys.* **90**, 015001 (2018).
58. Yan, B. & Felsner, C. Topological materials: Weyl semimetals. *Annu. Rev. Condens. Matter Phys.* **8**, 337–354 (2017).
59. Tian, J., Hong, S., Miotkowski, L., Datta, S. & Chen, Y. P. Observation of current-induced, long-lived persistent spin polarization in a topological insulator: a rechargeable spin battery. *Sci. Adv.* **3**, e1602531 (2017).
60. Mellnik, A. R. et al. Spin-transfer torque generated by a topological insulator. *Nature* **511**, 449–451 (2014).
61. Lin, B. C. et al. Electric control of Fermi arc spin transport in individual topological semimetal nanowires. *Phys. Rev. Lett.* **124**, 116802 (2020).
62. Chang, G. et al. Unconventional photocurrents from surface Fermi arcs in topological chiral semimetals. *Phys. Rev. Lett.* **124**, 166404 (2020).
63. Fu, L. Topological crystalline insulators. *Phys. Rev. Lett.* **106**, 106802 (2011).
64. Hsieh, T. H. et al. Topological crystalline insulators in the SnTe material class. *Nat. Commun.* **3**, 1–7 (2012).
65. Sancho, M. P. L., Sancho, J. M. L. & Rubio, J. Quick iterative scheme for the calculation of transfer matrices: application to Mo (100). *J. Phys. F* **14**, 1205 (1984).
66. Sancho, M. P. L., Sancho, J. M. L., Sancho, J. M. L. & Rubio, J. Highly convergent schemes for the calculation of bulk and surface Green functions. *J. Phys. F* **15**, 851 (1985).
67. Varnava, N. & Vanderbilt, D. Surfaces of axion insulators. *Phys. Rev. B* **98**, 245117 (2018).
68. Huang, D. & Hoffman, J. E. Monolayer FeSe on SrTiO_3 . *Annu. Rev. Condens. Matter Phys.* **8**, 311–336 (2017).
69. Kato, Y. K., Myers, R. C., Gossard, A. C. & Awschalom, D. D. Observation of the spin Hall effect in semiconductors. *Science* **306**, 1910–1913 (2004).
70. Saitoh, E., Ueda, M., Miyajima, H. & Tataru, G. Conversion of spin current into charge current at room temperature: inverse spin-Hall effect. *Appl. Phys. Lett.* **88**, 182509 (2006).
71. Valenzuela, S. O. & Tinkham, M. Direct electronic measurement of the spin Hall effect. *Nature* **442**, 176–179 (2006).
72. Kimura, T., Otani, Y., Sato, T., Takahashi, S. & Maekawa, S. Room-temperature reversible spin hall effect. *Phys. Rev. Lett.* **98**, 156601 (2007).
73. Hohenberg, P. & Kohn, W. Inhomogeneous electron gas. *Phys. Rev.* **136**, B864–B871 (1964).
74. Kohn, W. & Sham, L. J. Self-consistent equations including exchange and correlation effects. *Phys. Rev.* **140**, A1133–A1138 (1965).
75. Kresse, G. & Furthmüller, J. Efficiency of ab-initio total energy calculations for metals and semiconductors using a plane-wave basis set. *Comput. Mater. Sci.* **6**, 15–50 (1996).
76. Kresse, G. & Furthmüller, J. Efficient iterative schemes for ab initio total-energy calculations using a plane-wave basis set. *Phys. Rev. B* **54**, 11169–11186 (1996).
77. Perdew, J. P., Burke, K. & Ernzerhof, M. Generalized gradient approximation made simple. *Phys. Rev. Lett.* **77**, 3865–3868 (1996).
78. Blöchl, P. E. Projector augmented-wave method. *Phys. Rev. B* **50**, 17953–17979 (1994).
79. Mostofi, A. A. et al. An updated version of wannier90: a tool for obtaining maximally-localised Wannier functions. *Comput. Phys. Commun.* **185**, 2309–2310 (2014).
80. Laturia, A., Van de Put, M. L. & Vandenberghe, W. G. Dielectric properties of hexagonal boron nitride and transition metal dichalcogenides: from monolayer to bulk. *npj 2D Mater. Appl.* **2**, 1–7 (2018).

Acknowledgements

This work was supported by an Office of Naval Research MURI through grant #N00014-17-1-2661. We are grateful for the insightful suggestions by Dr. Zhurun Ji.

Author contributions

H.X. and J.L. conceived the idea and designed the project. H.X. derived the theories. H.X. performed the calculations and wrote the paper with the help of H.W. and J.Z. J.L. supervised the project. All authors analyzed the data and contributed to the discussions of the results.

Competing interests

The authors declare no competing interests.

Additional information

Supplementary information The online version contains supplementary material available at <https://doi.org/10.1038/s41467-021-24541-7>.

Correspondence and requests for materials should be addressed to J.L.

Peer review information *Nature Communications* thanks Jay Sau and the other, anonymous, reviewer(s) for their contribution to the peer review of this work. Peer reviewer reports are available.

Reprints and permission information is available at <http://www.nature.com/reprints>

Publisher's note Springer Nature remains neutral with regard to jurisdictional claims in published maps and institutional affiliations.



Open Access This article is licensed under a Creative Commons Attribution 4.0 International License, which permits use, sharing, adaptation, distribution and reproduction in any medium or format, as long as you give appropriate credit to the original author(s) and the source, provide a link to the Creative Commons license, and indicate if changes were made. The images or other third party material in this article are included in the article's Creative Commons license, unless indicated otherwise in a credit line to the material. If material is not included in the article's Creative Commons license and your intended use is not permitted by statutory regulation or exceeds the permitted use, you will need to obtain permission directly from the copyright holder. To view a copy of this license, visit <http://creativecommons.org/licenses/by/4.0/>.

© The Author(s) 2021

Supplementary Materials
to
Pure Spin Photocurrent in Non-centrosymmetric Crystals:
Bulk Spin Photovoltaic Effect

Haowei Xu¹, Hua Wang¹, Jian Zhou¹, and Ju Li^{1,2}

¹Department of Nuclear Science and Engineering, Massachusetts Institute of Technology,
Cambridge, Massachusetts 02139, USA

¹Department of Materials Science and Engineering, Massachusetts Institute of Technology,
Cambridge, Massachusetts 02139, USA

Table of Contents

1	Derivations of NLO spin current conductivity	2
2	Reproduce the shift and injection charge current formulae	6
2.1	NLO charge conductivities in the length gauge	6
2.2	Equivalence between the velocity gauge and the length gauge	8
3	Shift- and injection-like mechanisms for the spin current	10
3.1	\mathcal{P} -broken, \mathcal{T} -conserved systems	10
3.2	\mathcal{P} -broken, \mathcal{T} -broken, \mathcal{PT} -conserved systems	11
3.3	\mathcal{P} -broken, \mathcal{T} -broken, \mathcal{PT} -broken system	11

4	The definition of spin current	12
5	Experimental considerations	13
5.1	Estimation of the temperature rise	13
5.2	Maximum spin current density	14
5.3	Detection of the spin current	15
6	Computational benchmarks	15
6.1	Numerical comparison between the velocity gauge and length gauge	16
6.2	NLO conductivity as a function of lifetime τ	16
6.3	NLO conductivity as a function of SOC strength	18
7	NLO spin current under circularly polarized light	19

1 Derivations of NLO spin current conductivity

In this section we derive the NLO spin current conductivity from quadratic response theory, in a similar fashion to Refs. [1, 2]. The Hamiltonian of the system can be written as

$$H = H_0 + V \tag{S1}$$

where H_0 is the unperturbed Hamiltonian, while V is a perturbation, from e.g. the interaction between light and the electrons. Without the interaction term V , the equilibrium density matrix should be

$$\rho_0 = \frac{1}{Z} e^{-\beta H_0} \tag{S2}$$

Note that $[\rho_0, H_0] = 0$. When V is turned on, the equation of motion of the density matrix $\rho(t)$ should be (von Neumann equation)

$$\frac{\partial \rho}{\partial t} = -\frac{i}{\hbar} [H, \rho] - \frac{\rho - \rho_0}{\tau} \tag{S3}$$

The last term $-\frac{\rho - \rho_0}{\tau}$ is a dissipation that describes the interaction between the system and the heat bath: the system always has the tendency to return to ρ_0 . Here we adopted the constant relaxation time approximation and use a uniform τ for all states. In practice, τ should be different for different states (e.g., electrons and holes may have different τ). More rigorously, one should use $\frac{\partial \rho}{\partial t}|_{\text{col}}$, which

incorporates all relaxation processes, such the scattering of the electrons/holes with phonons, impurities, etc, and the spin relaxation process. But we made simplifications by using $\frac{\partial \rho}{\partial t}|_{\text{col}} \approx -\frac{\rho - \rho_0}{\tau}$.

In order to solve Eq. (S3), we use a trick similar to the transformation between the Schrodinger picture and the interaction picture. Let $\tilde{\rho}(t) = e^{\frac{t}{\tau}} e^{i\frac{H_0}{\hbar}t} \rho(t) e^{-i\frac{H_0}{\hbar}t}$, then we have

$$\begin{aligned} \frac{\partial \tilde{\rho}}{\partial t} &= \frac{1}{\tau} e^{\frac{t}{\tau}} e^{i\frac{H_0}{\hbar}t} \rho(t) e^{-i\frac{H_0}{\hbar}t} + i\frac{H_0}{\hbar} e^{\frac{t}{\tau}} e^{i\frac{H_0}{\hbar}t} \rho(t) e^{-i\frac{H_0}{\hbar}t} + e^{\frac{t}{\tau}} e^{i\frac{H_0}{\hbar}t} \frac{\partial \rho(t)}{\partial t} e^{-i\frac{H_0}{\hbar}t} + e^{\frac{t}{\tau}} e^{i\frac{H_0}{\hbar}t} \rho(t) \left(-i\frac{H_0}{\hbar}\right) e^{-i\frac{H_0}{\hbar}t} \\ &= e^{\frac{t}{\tau}} e^{i\frac{H_0}{\hbar}t} \left\{ \frac{\rho}{\tau} + \frac{i}{\hbar} [H_0, \rho] - \frac{i}{\hbar} [H, \rho] - \frac{\rho - \rho_0}{\tau} \right\} e^{-i\frac{H_0}{\hbar}t} \\ &= -\frac{i}{\hbar} [\tilde{V}, \tilde{\rho}] + \frac{\rho_0}{\tau} e^{\frac{t}{\tau}} \end{aligned} \tag{S4}$$

where $\tilde{V}(t) = e^{i\frac{H_0}{\hbar}t} V(t) e^{-i\frac{H_0}{\hbar}t}$. Then we can integrate Eq. (S4) to get

$$\begin{aligned} \tilde{\rho}(t) &= \tilde{\rho}(0) - \frac{i}{\hbar} \int_0^t dt' [\tilde{V}(t'), \tilde{\rho}(t')] + \frac{\rho_0}{\tau} \int_0^t dt' e^{\frac{t'}{\tau}} \\ &= \rho_0 + \rho_0 \left(e^{\frac{t}{\tau}} - 1 \right) - \frac{i}{\hbar} \int_0^t dt' [\tilde{V}(t'), \tilde{\rho}(t')] \\ &= \rho_0 e^{\frac{t}{\tau}} - \frac{i}{\hbar} \int_0^t dt' [\tilde{V}(t'), \tilde{\rho}(t')] \\ &= \rho_0 e^{\frac{t}{\tau}} - \frac{i}{\hbar} \int_0^t dt' \left[\tilde{V}(t'), \rho_0 e^{\frac{t'}{\tau}} - \frac{i}{\hbar} \int_0^{t'} dt'' [\tilde{V}(t''), \tilde{\rho}(t'')] \right] \\ &= \rho_0 e^{\frac{t}{\tau}} - \frac{i}{\hbar} \int_0^t dt' [\tilde{V}(t'), \rho_0 e^{\frac{t'}{\tau}}] - \frac{i}{\hbar} \int_0^t dt' \left[\tilde{V}(t'), -\frac{i}{\hbar} \int_0^{t'} dt'' [\tilde{V}(t''), \tilde{\rho}(t'')] \right] \\ &= \dots \end{aligned} \tag{S5}$$

By iteratively putting $\tilde{\rho}(t)$ into the bracket on the rightmost of the equation above, we can obtain

$$\tilde{\rho}(t) = \tilde{\rho}^{(0)}(t) + \tilde{\rho}^{(1)}(t) + \tilde{\rho}^{(2)}(t) + \dots \tag{S6}$$

with

$$\begin{aligned} \tilde{\rho}^{(0)}(t) &= \rho_0 e^{\frac{t}{\tau}} \\ \tilde{\rho}^{(n+1)}(t) &= -\frac{i}{\hbar} \int_0^t dt' [\tilde{V}(t'), \tilde{\rho}^{(n)}(t')] \end{aligned} \tag{S7}$$

Then going back from $\tilde{\rho}(t)$ to $\rho(t)$ with $\rho(t) = e^{-\frac{t}{\tau}} e^{-i\frac{H_0}{\hbar}t} \tilde{\rho}(t) e^{i\frac{H_0}{\hbar}t}$, we have

$$\rho(t) = \rho^{(0)}(t) + \rho^{(1)}(t) + \rho^{(2)}(t) + \dots \tag{S8}$$

with

$$\rho^{(0)} = \rho_0 \tag{S9}$$

and

$$\begin{aligned}
\rho^{(n+1)}(t) &= e^{-\frac{t}{\tau}} e^{-i\frac{H_0}{\hbar}t} \tilde{\rho}^{(n+1)}(t) e^{i\frac{H_0}{\hbar}t} \\
&= -\frac{i}{\hbar} \int_0^t dt' e^{-\frac{t'}{\tau}} e^{-i\frac{H_0}{\hbar}t'} [\tilde{V}(t'), \tilde{\rho}^{(n)}(t')] e^{i\frac{H_0}{\hbar}t} \\
&= -\frac{i}{\hbar} \int_0^t dt' e^{-\frac{t-t'}{\tau}} e^{-i\frac{H_0}{\hbar}(t-t')} [V(t'), \rho^{(n)}(t')] e^{i\frac{H_0}{\hbar}(t-t')} \\
&= \frac{i}{\hbar} \int_0^t dt' e^{-\frac{t'}{\tau}} e^{-i\frac{H_0}{\hbar}t'} [V(t-t'), \rho^{(n)}(t-t')] e^{i\frac{H_0}{\hbar}t'}
\end{aligned} \tag{S10}$$

Next we expand $V(t-t')$ with a Fourier transformation $V(t-t') = \int \frac{d\omega}{2\pi} V(\omega) e^{i\omega(t-t')}$. Then $\rho^{(1)}$ can be calculated as

$$\begin{aligned}
\rho_{nm}^{(1)}(t) &= \langle n | \rho^{(1)}(t) | m \rangle \\
&= \frac{i}{\hbar} \int_0^t dt' \langle n | e^{-\frac{t'}{\tau}} e^{-i\frac{H_0}{\hbar}t'} [V(t-t'), \rho_0] e^{i\frac{H_0}{\hbar}t'} | m \rangle \\
&= \frac{i}{\hbar} \int \frac{d\omega}{2\pi} \langle n | [V(\omega), \rho_0] | m \rangle e^{i\omega t} \int_0^t dt \exp\left(\frac{i}{\hbar} \left[(E_m - E_n) + \frac{i\hbar}{\tau} - \hbar\omega \right] t\right) \\
&= \frac{i}{\hbar} \int \frac{d\omega}{2\pi} V_{nm}(\omega) (f_{mm} - f_{nn}) e^{i\omega t} \frac{\exp\left(\frac{i}{\hbar} \left[(E_m - E_n) + \frac{i\hbar}{\tau} - \hbar\omega \right] t\right) - 1}{\frac{i}{\hbar} \left[(E_m - E_n) + \frac{i\hbar}{\tau} - \hbar\omega \right]} \\
&= \int \frac{d\omega}{2\pi} e^{i\omega t} \frac{f_{nm} V_{nm}(\omega)}{E_{mn} - \hbar\omega + \frac{i\hbar}{\tau}}
\end{aligned} \tag{S11}$$

Obviously,

$$\rho_{nm}^{(1)}(\omega; \omega) = \frac{f_{nm} V_{nm}(\omega)}{E_{mn} - \hbar\omega + \frac{i\hbar}{\tau}} \tag{S12}$$

Then, the second order $\rho^{(2)}$

$$\begin{aligned}
\rho_{nm}^{(2)}(t) &= \langle n | \rho^{(2)}(t) | m \rangle \\
&= \frac{i}{\hbar} \int \frac{d\omega'}{2\pi} e^{i\omega' t} \int_0^t dt' \exp\left(\frac{i}{\hbar} \left[(E_m - E_n) + \frac{i\hbar}{\tau} - \hbar\omega' \right] t'\right) \sum_l \left(V_{nl}(\omega') \rho_{lm}^{(1)}(t-t') - \rho_{nl}^{(1)}(t-t') V_{lm}(\omega') \right) \\
&= \int \frac{d\omega}{2\pi} \int \frac{d\omega'}{2\pi} e^{i(\omega+\omega')t} \frac{1}{E_{mn} - \hbar(\omega+\omega') + \frac{i\hbar}{\tau}} \sum_l \left(\frac{f_{lm} V_{nl}(\omega') V_{lm}(\omega)}{E_{ml} - \hbar\omega + \frac{i\hbar}{\tau}} - \frac{f_{nl} V_{nl}(\omega) V_{lm}(\omega')}{E_{ln} - \hbar\omega + \frac{i\hbar}{\tau}} \right)
\end{aligned} \tag{S13}$$

We have

$$\rho_{nm}^{(2)}(\omega + \omega'; \omega, \omega') = \frac{1}{E_{mn} - \hbar(\omega + \omega') + \frac{i\hbar}{\tau}} \sum_l \left(\frac{f_{lm} V_{nl}(\omega') V_{lm}(\omega)}{E_{ml} - \hbar\omega + \frac{i\hbar}{\tau}} - \frac{f_{nl} V_{nl}(\omega) V_{lm}(\omega')}{E_{ln} - \hbar\omega + \frac{i\hbar}{\tau}} \right) \tag{S14}$$

For an arbitrary operator θ , the thermal expectation value of θ should be

$$\langle \theta \rangle = \text{Tr}(\theta \rho) \tag{S15}$$

The first order response is

$$\begin{aligned}\langle\theta\rangle^{(1)}(\omega;\omega) &= \int \frac{d\mathbf{k}}{(2\pi)^3} \sum_{mn} \theta_{mn} \rho_{nm}^{(1)}(\omega;\omega) \\ &= \int \frac{d\mathbf{k}}{(2\pi)^3} \sum_{mn} \frac{f_{nm} \theta_{mn} V_{nm}(\omega)}{E_{nm} - \hbar\omega + \frac{i\hbar}{\tau}}\end{aligned}\quad (\text{S16})$$

The the second order response is

$$\begin{aligned}\langle\theta\rangle^{(2)}(\omega + \omega'; \omega, \omega') &= \int \frac{d\mathbf{k}}{(2\pi)^3} \sum_{mn} \theta_{mn} \rho_{nm}^{(2)}(\omega + \omega'; \omega, \omega') \\ &= \int \frac{d\mathbf{k}}{(2\pi)^3} \sum_{mnl} \frac{\theta_{mn}}{E_{mn} - \hbar(\omega + \omega') + \frac{i\hbar}{\tau}} \left(\frac{f_{lm} V_{nl}(\omega') V_{lm}(\omega)}{E_{ml} - \hbar\omega + \frac{i\hbar}{\tau}} - \frac{f_{nl} V_{nl}(\omega) V_{lm}(\omega')}{E_{ln} - \hbar\omega + \frac{i\hbar}{\tau}} \right) \\ &= \int \frac{d\mathbf{k}}{(2\pi)^3} \sum_{mnl} \frac{f_{lm} V_{lm}(\omega)}{E_{ml} - \hbar\omega + \frac{i\hbar}{\tau}} \left(\frac{\theta_{mn} V_{nl}(\omega')}{E_{mn} - \hbar(\omega + \omega') + \frac{i\hbar}{\tau}} - \frac{V_{mn}(\omega') \theta_{nl}}{E_{nl} - \hbar(\omega + \omega') + \frac{i\hbar}{\tau}} \right)\end{aligned}\quad (\text{S17})$$

The last equity can be obtained with an interchange of dummy variables as ($n \rightarrow l, l \rightarrow m, m \rightarrow n$). For the nonlinear spin current effect, the interaction is

$$\begin{aligned}V(\omega) &= -e \sum_{i=1}^N \mathbf{v}_i \cdot \mathbf{A}(\omega) \\ &= \frac{ie}{\omega} \sum_{i=1}^N \mathbf{v}_i \cdot \mathcal{E}(\omega)\end{aligned}\quad (\text{S18})$$

where \mathbf{A} is the vector potential while \mathcal{E} is the electric field. After a second quantization, we have $V_{nm}(\omega)$ in the basis of Bloch waves

$$V_{nm}(\omega) = \frac{ie}{\omega} v_{nm}^b \mathcal{E}_b(\omega) \quad (\text{S19})$$

For the spin current in the a direction with spin component i , we should have $\theta_{nm} = j_{nm}^{a,i} = \frac{1}{2} \{v^a, s^i\}_{nm}$, where $s^i = \frac{\hbar}{2} \sigma^i$ is the spin operator.

Finally, the nonlinear direct spin current is

$$\langle j^{a,s^i} \rangle^{(2)}(0; \omega, -\omega) = -\frac{e^2}{\omega^2} \int \frac{d\mathbf{k}}{(2\pi)^3} \sum_{mnl} \frac{f_{lm} v_{lm}^b}{E_{ml} - \hbar\omega + \frac{i\hbar}{\tau}} \left(\frac{j_{mn}^{a,s^i} v_{nl}^c}{E_{mn} + \frac{i\hbar}{\tau}} - \frac{v_{mn}^c j_{nl}^{a,s^i}}{E_{nl} + \frac{i\hbar}{\tau}} \right) \mathcal{E}_b(\omega) \mathcal{E}_c(-\omega) \quad (\text{S20})$$

And the spin conductivity can be written as

$$\sigma_{bc}^{a,s^i}(0; \omega, -\omega) = -\frac{e^2}{\hbar^2 \omega^2} \int \frac{d\mathbf{k}}{(2\pi)^3} \sum_{mnl} \frac{f_{lm} v_{lm}^b}{\omega_{ml} - \omega + \frac{i}{\tau}} \left(\frac{j_{mn}^{a,s^i} v_{nl}^c}{\omega_{mn} + \frac{i}{\tau}} - \frac{v_{mn}^c j_{nl}^{a,s^i}}{\omega_{nl} + \frac{i}{\tau}} \right) \quad (\text{S21})$$

where we have replaced E_{mn} with $\hbar\omega_{mn}$. Eq. (S21) is exactly the same as Eq. (2) in the main text.

2 Reproduce the shift and injection charge current formulae

2.1 NLO charge conductivities in the length gauge

In Sec. 1, we adopted the so-called *velocity* gauge in deriving the NLO spin/charge conductivity, where the interaction with the oscillating electric field is described by the vector potential and velocity as in Eq. (S18). A charge current version of Eq. (S21), where one sets $j^{a,s^0} = ev^a$

$$\sigma_{bc}^a(0; \omega, -\omega) = -\frac{e^3}{\hbar^2\omega^2} \int \frac{d\mathbf{k}}{(2\pi)^3} \sum_{mnl} \frac{f_{lm}v_{lm}^b}{\omega_{ml} - \omega + \frac{i}{\tau}} \left(\frac{v_{mn}^a v_{nl}^c}{\omega_{mn} + \frac{i}{\tau}} - \frac{v_{mn}^c v_{nl}^a}{\omega_{nl} + \frac{i}{\tau}} \right) \quad (\text{S22})$$

has been derived in Refs. [1, 2] and has been used in e.g. Refs. [3, 4]. On the other hand, a different version of the formulae [5] for calculating the NLO charge conductivity, which uses the *length* gauge, seems more popular in literatures. In the length gauge, the interaction with light is described by $V = -er \cdot \mathcal{E}$, where r is the position (length) operator. We first give a brief description on the formulae in length gauge, and then show that they are equivalent with our Eq. (S22).

In a time reversal symmetric system, the NLO charge current is divided into two parts, namely the *shift* current and the *injection* current,

$$\begin{aligned} j_{\text{shift}}^a &= 2\zeta_{bc}^a(0; \omega, -\omega) E^b(\omega) E^c(-\omega) \\ \frac{dj_{\text{circular}}^a}{dt} &= 2\eta_{bc}^a(0; \omega, -\omega) E^b(\omega) E^c(-\omega) \end{aligned} \quad (\text{S23})$$

The shift current conductivity is

$$\zeta_{bc}^a(0; \omega, -\omega) = -\frac{i\pi e^3}{2\hbar^2} \int_{BZ} \frac{d^3\mathbf{k}}{(2\pi)^3} \sum_{n,m} f_{nm} (r_{mn}^b r_{nm;a}^c + r_{mn}^c r_{nm;a}^b) \delta(\omega_{mn} - \omega) \quad (\text{S24})$$

where

$$r_{nm;a}^b = \frac{\partial r_{nm}^a}{\partial k^b} - i[\xi_{nn}^b - \xi_{mm}^b] r_{nm}^a \quad (\text{S25})$$

is the generalized derivative of position operator r with respect to k and $\xi_{nn}^a = i\langle u_{nk} | \partial_{k^a} | u_{nk} \rangle$, where $|u_{nk}\rangle$ is the cell-periodic part of the wavefunction $|nk\rangle$. Note that for Bloch waves, it is not straightforward to define the full matrix of the position operator $r_{mn} = \langle m | r | n \rangle$, since the Bloch waves are infinite

in space. Usually r_{mn} is defined with only the interband elements

$$r_{mn} = \begin{cases} \frac{v_{mn}}{i\omega_{mn}}, & m \neq n \\ 0, & m = n \end{cases} \quad (\text{S26})$$

But the definition of ξ is valid for intraband elements with $m = n$ as well.

Under a linearly polarized light $b = c$, Eq. (S24) can be further simplified as

$$\sigma_{bb}^a(0; \omega, -\omega) = -\frac{\pi e^3}{2\hbar^2} \int_{BZ} \frac{d^3\mathbf{k}}{(2\pi)^3} \sum_{n,m} f_{nm} R_{nm}^a |r_{nm}^b|^2 \delta(\omega_{mn} - \omega) \quad (\text{S27})$$

where

$$r_{nm}^b = |r_{nm}^b| e^{-i\phi_{nm}}$$

and

$$R_{nm}^a = \frac{\partial \phi_{nm}}{\partial k^a} + \xi_{nn}^a - \xi_{mm}^a$$

is called the *shift vector*.

The injection current response function is

$$\eta_{bc}^a(0; \omega, -\omega) = \frac{\pi e^3}{2\hbar^2} \int_{BZ} \frac{d^3\mathbf{k}}{(2\pi)^3} \sum_{n,m} f_{nm} \Delta_{nm}^a [r_{mn}^c, r_{nm}^b] \delta(\omega_{mn} - \omega) \quad (\text{S28})$$

where $\Delta_{nm}^a = v_{nn}^a - v_{mm}^a$ and $[r_{mn}^c, r_{nm}^b] = r_{mn}^c r_{nm}^b - r_{mn}^b r_{nm}^c$.

The shift current can be induced by a linearly polarized light ($b = c$), and is a static current. On the other hand, the injection current cannot be induced by a linearly polarized light, and it should grow with time, thus it is somewhat like *injected* into the system. If the carrier lifetime is τ , then there should be a dissipation term $-j_{\text{injection}}/\tau$. And in the static limit ($t \rightarrow \infty$),

$$j_{\text{injection}} = 2\tau \eta_{bc}^a(0; \omega, -\omega) E^b(\omega) E^c(-\omega) \quad (\text{S29})$$

so the *effective* conductivity should be defined as $\tau \eta_{bc}^a(0; \omega, -\omega)$. Eqs. (S24, S28) are derived in Ref. [5] and is widely used in many papers.

Here we would like to remark that the physical mechanism of the shift current and injection current are more evident in the length gauge format. Eqs. (S27, S28) are reminiscent of the Fermi's golden rule. The Dirac functions indicate that light induces resonant interband transitions, and the transition rate are proportional to $|r_{mn}^b|^2$ for LPL, and $[r_{mn}^c, r_{nm}^b]$ for CPL. Then the shift current comes from the fact that the wavefunction centers of electrons and holes differ by a factor of R_{nm}^a , which leads to a electric dipole eR_{nm}^a . The time derivative of the electric dipole is the current. On the other hand,

the injection current comes from the fact that the electrons and holes have different velocities, and the net current is determined by the velocity difference $\Delta_{nm}^a = v_{nn}^a - v_{mm}^a$.

2.2 Equivalence between the velocity gauge and the length gauge

Eq. (S22) and Eqs. (S24, S28) look very different, but they should give the same result in cases that they are both applicable, because they are dealing with the same physical problem: the charge current generated under light illumination. The difference is that, Eq. (S22) uses the velocity gauge and the light coupling with the system is included by replacing \mathbf{p} with $\mathbf{p} - \frac{e}{c}\mathbf{A}$, where \mathbf{p} is the momentum operator and \mathbf{A} is the vector potential. Whereas Eqs. (S24, S28) use the length gauge and the light interaction is included by an additional term in the Hamiltonian $H_{\text{int}} = -e\mathbf{r} \cdot \mathbf{E}$, where \mathbf{r} is the position operator and \mathbf{E} is the electric field. These approaches should be equivalent and lead to the same results, as discussed in e.g. Refs. [6, 7].

Both velocity gauge and length gauge are applicable regardless time reversal symmetry \mathcal{T} . However, in deriving Eqs. (S24, S28), Ref. [5] assumed a \mathcal{T} -conserved system and made some simplifications. Thus Eqs. (S24, S28) are not valid when \mathcal{T} is broken. In the following, we would show that Eq. (S22) and Eqs. (S24, S28) are equivalent in a \mathcal{T} -conserved system. Specifically, under LPL, one should consider the symmetric real part of Eq. (S22), which is equivalent to the shift current as in Eqs. (S24), while under CPL, one should consider the asymmetric imaginary part of Eq. (S22), which corresponds to the injection current as in Eqs. (S28).

In order to show the equivalence, the first step is to factorize the denominator of Eq. (S22) with Sokhotski-Plemelj Formula. That is, in the limit of $\tau \rightarrow \infty$ ($\delta = 1/\tau \rightarrow 0$), one has¹

$$\begin{aligned} D_1 &= \frac{1}{\omega_{mn} + i\delta} = \frac{P}{\omega_{mn}} - i\pi\delta(\omega_{mn}) \\ D_2 &= \frac{1}{\omega_{ml} - \Omega + i\delta} = \frac{P}{\omega_{ml} - \Omega} - i\pi\delta(\omega_{ml} - \Omega) \end{aligned} \quad (\text{S30})$$

here $\delta(x)$ is the Dirac delta function and P stands for the Cauchy principal value in \mathbf{k} integration.

The next step is to rearrange the numerator of Eq. (S22), which is $N^{0abd}(\mathbf{k}) = v^a(\mathbf{k})v^b(\mathbf{k})v^c(\mathbf{k})$, according to their behavior under \mathcal{T} operation. As discussed in the main text, one has $\mathcal{T}N^{0abd}(\mathbf{k}) = -N^{0abd*}(-\mathbf{k})$. Since the denominator is invariant under \mathcal{T} , one has $\frac{N^{0abd}(\mathbf{k})}{D_1(\mathbf{k})D_2(\mathbf{k})} = -\frac{N^{0abd*}(-\mathbf{k})}{D_1(-\mathbf{k})D_2(-\mathbf{k})}$. Consequently, after a summation over $\pm\mathbf{k}$, only the imaginary part of $N^{0abd}(\mathbf{k})$ would contribute to the final result, and thus we can ignore the real part of $N^{0abd}(\mathbf{k})$ and treat it as a purely imaginary quantity.

Reproduce the shift current. First, we note that the a dc current should be a real quantity.

¹Here we focus on the first term in the bracket of Eq. (S22), the second term can be analyzed in the same fashion.

For a LPL, E^b and E^c has no phase difference and only the real part of the conductivity σ_{bc}^a contributes to the NLO current. As discussed above, the numerator $N^{0abd}(\mathbf{k})$ can be treated as a purely imaginary quantity, thus one needs to consider the imaginary part of the denominator, which is

$$\text{Im}(D_1 D_2) = \pi \frac{P}{\omega_{mn}} \delta(\omega_{ml} - \Omega) + \pi \frac{P}{\omega_{ml} - \hbar\Omega} \delta(\omega_{mn}) \quad (\text{S31})$$

The second term in symmetric with respect to the permutation of m, n (after summation over m, n), while the imaginary part of $v_{nl}^a v_{lm}^b v_{mn}^c$ is asymmetric with respect to m, n . Therefore only the first term in Eq. (S31) would not vanish in the final result. Now it's straightforward to check that that the integrand in Eq. (S22) is terms with format

$$\sum_{mnl} \frac{f_{lm} v_{lm}^b}{\omega_{ml}^2} \left(\frac{v_{mn}^a v_{nl}^c}{\omega_{mn}} - \frac{v_{mn}^c v_{nl}^a}{\omega_{nl}} \right) \delta(\omega_{ml} - \omega) \quad (\text{S32})$$

where we have replaced ω in the prefactor of Eq. (S22) with ω_{ml} because of the the delta function.

On the other hand, the integrand of Eq. (S24) is

$$\sum_{ml} f_{lm} (r_{ml}^b r_{lm;a}^c + r_{ml}^c r_{lm;a}^b) \delta(\omega_{ml} - \omega) \quad (\text{S33})$$

The equivalence between Eq. (S32) and Eq. (S33) can be proved by using Eq. (S26) and plugging in the *sum rule* for $r_{lm;a}^b$ [8]

$$r_{lm;a}^b = \frac{r_{lm}^a \Delta_{ml}^b + r_{lm}^b \Delta_{ml}^a}{\omega_{lm}} + \frac{i}{\omega_{lm}} \sum_n (\omega_{nm} r_{ln}^a r_{nm}^b - \omega_{ln} r_{ln}^b r_{nm}^a) \quad (\text{S34})$$

Note that the first term in Eq. (S34), $F_{lm;a}^b = \frac{r_{lm}^a \Delta_{ml}^b + r_{lm}^b \Delta_{ml}^a}{\omega_{lm}}$, does not contribute to the final result because $f_{lm} r_{ml}^c F_{lm;a}^b$ is asymmetric in m, l .

Reproduce the injection current. For a circularly polarized light, E^b and E^c should have a phase difference of i . In order to get a real current, we need to consider the imaginary part of σ_{bc}^a . In this case we need to examine the real part of the denominator of Eq. (S22), which is

$$\text{Re}(D_1 D_2) = \frac{P}{\omega_{mn}(\omega_{ml} - \Omega)} - \pi^2 \delta(\omega_{mn}) \delta(\omega_{ml} - \Omega) \quad (\text{S35})$$

One can see that the first and second term in Eq. (S35) corresponds to $m \neq n$ and $m = n$, respectively. In case that $\tau \rightarrow 0$, the contribution from the first term is much smaller than the second term and thus we only consider the second term.

Putting $m = n$ ($n = l$) in the first (second) term of Eq. (S22), one has the integrand as

$$\begin{aligned}
& -i\tau \sum_{ml} \frac{f_{lm} v_{lm}^b v_{ml}^c}{\omega_{ml}^2} (v_{mm}^a - v_{ll}^a) \delta(\omega_{ml} - \omega) \\
& = i\tau \sum_{ml} f_{lm} (v_{mm}^a - v_{ll}^a) r_{lm}^b r_{ml}^c \delta(\omega_{ml} - \omega) \\
& \rightarrow \frac{i\tau}{2} \sum_{ml} f_{lm} \Delta_{ml}^a [r_{lm}^b, r_{ml}^c] \delta(\omega_{ml} - \omega)
\end{aligned} \tag{S36}$$

In the last step we have taken the asymmetry part ($bc \leftrightarrow -cb$) of the integrand. One can see that Eq. (S36) is the same as the integrand of Eq. (S28) plus a τ factor, as expected.

3 Shift- and injection-like mechanisms for the spin current

As discussed in Sec. 2, the well-known shift and injection formulae in a \mathcal{T} -conserved system can be reproduced from the charge current part ($j^{a,s^0} = ev^a$) of Eq. (S21). In this section, we would show that for the spin current with $j^{a,s^i} = \frac{1}{2}\{v^a, s^i\}$, $i \neq 0$, Eq. (S21) can also be broken down into *shift*-like and *injection*-like parts. By shift- (injection-) like, we mean that the conductivity scale with τ^0 (τ^1), where τ is the carrier relaxation time.

3.1 \mathcal{P} -broken, \mathcal{T} -conserved systems

We first study a \mathcal{T} -conserved system. As in Sec. 2, we still need to factorize the denominator of Eq. (S21) with Eq. (S30), and the arrange the numerator according to its behavior under \mathcal{T} operation. Unlike $N^{0abd}(\mathbf{k})$, for the spin current, one has $\mathcal{T}N^{iabd}(\mathbf{k}) = N^{iabd*}(-\mathbf{k})$. Consequently, after a summation over $\pm\mathbf{k}$, only the *real* part of $N^{iabd}(\mathbf{k})$ contributes to the total conductivity, in contrast to the charge current, where the *imaginary* part of $N^{0abd}(\mathbf{k})$ contributes.

Linearly polarized light. Under a LPL, for the spin current one needs to consider the real part of the denominator, as in Eq. (S35). And similar algebra to that in Eq. (S36) leads to a integrand for the NLO spin conductivity as

$$\begin{aligned}
& i\tau \sum_{ml} f_{lm} \left(j_{mm}^{a,s^i} - j_{ll}^{a,s^i} \right) r_{lm}^b r_{ml}^c \delta(\omega_{ml} - \omega) \\
& \rightarrow \frac{i\tau}{2} \sum_{ml} f_{lm} \left(j_{mm}^{a,s^i} - j_{ll}^{a,s^i} \right) \{r_{lm}^b, r_{ml}^c\} \delta(\omega_{ml} - \omega)
\end{aligned} \tag{S37}$$

where we have taken the symmetry part ($bc \leftrightarrow cb$) as $\{r_{lm}^b, r_{ml}^c\} = r_{lm}^b r_{ml}^c + r_{lm}^c r_{ml}^b$ because we are dealing with LPL. One can see that for a \mathcal{T} -conserved system under LPL, the mechanism for spin current generation is actually *injection*-like. A prominent feature is that the NLO spin conductivity is (approximately) proportional to the lifetime τ .

Circularly polarized light. Under LPL, one needs to keep the imaginary part of the denominator as in Eq. (S31). This time the second term in Eq. (S31) would also contribute to the final result because the real part of $j_{nl}^{a,s^i} v_{lm}^b v_{mn}^c$ is also symmetric in m, n . As a result, under CPL, the contribution to the spin current has a *shift*-like part,

$$\sum_{mnl} \frac{f_{lm} v_{lm}^b}{\omega_{ml}^2} \left(\frac{j_{mn}^{a,s^i} v_{nl}^c}{\omega_{mn}} - \frac{v_{mn}^c j_{nl}^{a,s^i}}{\omega_{nl}} \right) \delta(\omega_{ml} - \omega) \quad (\text{S38})$$

which is independent of τ , plus a *injection*-like part

$$-i\tau \sum_{ml} \frac{f_{lm} v_{lm}^b v_{ml}^c}{(\omega_{ml} - \omega)\omega^2} \left(j_{mm}^{a,s^i} - j_{ll}^{a,s^i} \right) \quad (\text{S39})$$

which depends linearly on τ .

3.2 \mathcal{P} -broken, \mathcal{T} -broken, \mathcal{PT} -conserved systems

For a \mathcal{PT} -conserved system, one needs to study the imaginary part of $N^{iabd}(\mathbf{k})$ because $\mathcal{PT}N^{iabd}(\mathbf{k}) = -\tilde{N}^{iabd*}(-\mathbf{k})$. With similar analysis as in the previous section for \mathcal{T} -conserved system, one can find that the generation of spin current under LPL (CPL) has shift (injection)-like mechanism, respectively.

The same analysis also applies to charge current in a \mathcal{PT} -conserved system, and the results are listed in Table 2 of the main text.

3.3 \mathcal{P} -broken, \mathcal{T} -broken, \mathcal{PT} -broken system

In this kind of systems, both the real and imaginary parts of $N^{iabd}(\mathbf{k})$ can contribute to the conductivity for spin and charge currents. As a result, under either LPL or CPL, the shift- and injection-like mechanisms would both contribute.

4 The definition of spin current

There are lots of debates on the definition of the spin current. In the main text we adopted the conventional definition $j_1 = \frac{1}{2}(vs + sv)$. But this definition is not entirely correct, although it is convenient, physically appealing, and extensively employed in many works until today. For example, this spin current is not conserved. Also, as suggested in Rashba's work [9], this definition would lead to a non-zero spin current even if an inversion asymmetric insulator is in equilibrium (under no electric field, light, etc.). There are lots of debates, and there are also works claiming that we do not need to modify this definition. See e.g., Ref. [10].

In Ref. [11], the authors proposed another definition, which is $j_2 = \frac{d(rs)}{dt}$. This definition can be conserved in some systems. However, it requires that "spin generation in the bulk is absent due to symmetry reasons". In other words, it requires the bulk integration $\frac{1}{V} \int dV \mathcal{T}(r) = 0$, where $\mathcal{T}(r)$ is the torque density on the spins. Unfortunately, this is not true under external light, which is necessary for our bulk spin photovoltaic effect. An intuitive picture is, under a circularly polarized light, the angular momentum of the photons can be transferred into the electron system, which obviously leads to $\frac{1}{V} \int dV \mathcal{T}(r) \neq 0$. Therefore, the definition of $j_2 = \frac{d(rs)}{dt}$ is also not perfectly correct if the system is under light illumination. Particularly, under strong light, the non-conservation of $j_2 = \frac{d(rs)}{dt}$ might be high. On the other hand, the calculation of the spin current with $j_2 = \frac{d(rs)}{dt}$ is rather involved in practice (although this definition looks simple). To the best of our knowledge, this definition has only been applied in simple model systems, and to the linear order response.

Here we roughly estimate the difference between the spin current defined with $j_1 = \frac{1}{2}(vs + sv)$ and $j_2 = \frac{d(rs)}{dt}$. Compared with j_1 , j_2 has an additional term that comes from the torque on the spins [11, 12]. This term is proportional to $[H, s]$. Therefore, the relative difference $\left| \frac{j_2 - j_1}{j_1} \right|$ can be roughly estimated from $\alpha_i = \frac{\|[H, s^i]\|}{\|H\| \cdot \|s^i\|}$, where $\|\cdot\|$ indicates matrix norm. This can be naively understood in the following way. We have $j_2 = \frac{d(rs)}{dt} = \frac{dr}{dt}s + \frac{ds}{dt}r = \frac{1}{2}\{[H, r], s\} + \frac{1}{2}\{r, [H, s]\}$, where $\{a, b\} = ab + ba$ ensures hermiticity. The first term is just j_1 , while the second term comes from the torque on the spins. The ratio between these two terms is (very roughly) $\alpha_i = \frac{\|[H, s^i]\|}{\|H\| \cdot \|s^i\|}$. Rigorously speaking, the position operator r needs extra care in infinite solid-state systems.

We have calculated and plotted α_z in the first Brillouin zone for MoS₂ (Figure S1a) and MnBi₂Te₄ (Figure S1b). One can see that α is on the order of 0.1 \sim 0.2. From this point of view, one may deduce that the difference between j_1 and j_2 is indeed not negligible, but in general cases, it would not qualitatively change the main results.

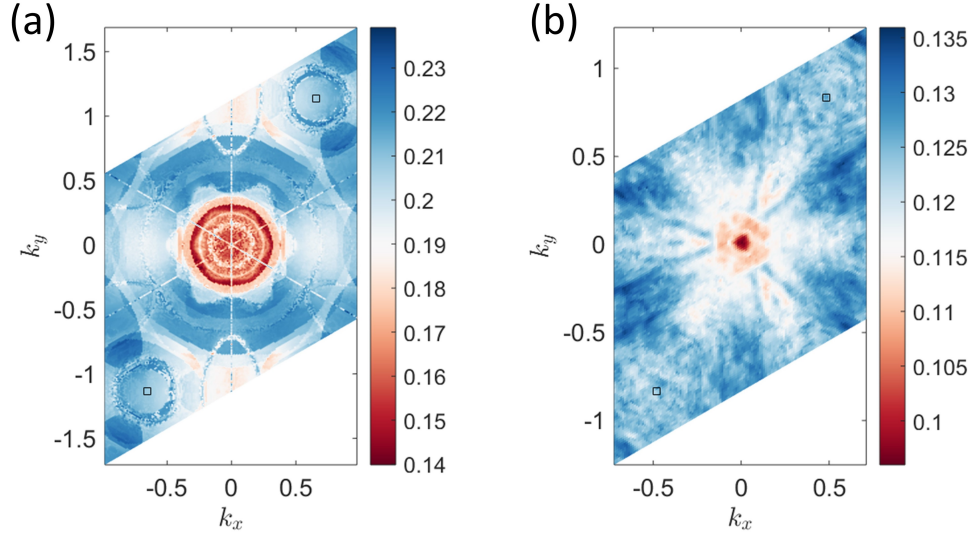


Figure S1: $\alpha_z = \frac{\|H, s^z\|}{\|H\| \cdot \|s^z\|}$ for (a) MoS₂ and (b) MnBi₂Te₄. The black boxes indicate K/K' points in the Brillouin zone.

5 Experimental considerations

5.1 Estimation of the temperature rise

For spin current generation, the temperature rise due to the energy dissipation is generally not significant. Here we take monolayer MoS₂ as an example. For the bulk spin photovoltaic effect studied in this work, the main energy consumption is the photon absorption due to interband transitions (electron-hole pair generation), and the absorbance is $A = 1 - \exp\left[-\frac{\omega}{c\epsilon_0}\epsilon^i(\omega)d\right] \approx \frac{\sigma^r(\omega)}{c\epsilon_0}d$, where ϵ_0 is the vacuum permittivity, ϵ_i is the imaginary part of the dielectric function, σ^r is the real part of the optical conductivity. d is the thickness of the material, which is taken as 0.6 nm for MoS₂. The energy consumption rate per unit area is

$$P = AI = \frac{\sigma^r(\omega)}{c\epsilon_0}d\frac{\epsilon_0 c}{2}E^2 = \frac{\sigma^r(\omega)d}{2}E^2 \quad (\text{S40})$$

where $I = \frac{\epsilon_0 c}{2}E^2$ is the intensity of the light. From our ab initio calculations, at $\omega = 3$ eV one has $\sigma^r(\omega) = 4 \times 10^5 \Omega/\text{m}$. In the main text, we showed that light with electric field strength on the order of $E = 100$ V/m would be able to generate a detectable spin current. With this field strength the energy absorption power is $P = 1.2 \times 10^{-4}$ W/cm², which is rather small. Here we calculate the temperature rise under an electric field of $E = 1$ MV/m, which is much larger, but readily available with laser technology. At this field strength, one has $P = 1.2 \times 10^4$ W/cm². Assume that MoS₂ is put on a

substrate with thermal conductivity κ and thickness l_{subs} . If a continuous wave (CW) light is used, then the steady steady-state temperature rise can be roughly estimated from

$$\Delta T_{\text{CW}} = \frac{P}{\kappa} l_{\text{subs}} \quad (\text{S41})$$

Assuming that $l_{\text{subs}} = 1 \mu\text{m}$ and $\kappa = 100 \text{ W} \cdot \text{m}^{-1} \cdot \text{K}^{-1}$, then $\Delta T_{\text{CW}} \approx 1.2 \text{ K}$, which is not significant. On the other hand, if a pulse laser is used, then the temperature rise can be estimated from

$$\Delta T_{\text{pulsed}} = \frac{\tau_{\text{pulse}} P S}{k_B} \quad (\text{S42})$$

Where S is the area of a unit-cell, k_B is the Boltzmann constant, while τ_{pulse} is the duration of the pulse, and is taken as 1 ps here. One can find that $\Delta T_{\text{pulsed}} \approx 0.7 \text{ K}$, which is also not significant as well.

We would like to note that, not all energies absorbed by the materials goes to the phonon (lattice) system. They may be re-emitted as photons when e.g., electrons and holes recombine. Therefore, the temperature rise in the ion system may be even lower than ΔT_{CW} and ΔT_{pulsed} estimated above.

5.2 Maximum spin current density

With the MoS₂ parameters, when the external field strength is $E = 1 \text{ MV/m}$, the spin current density is $10^8 \frac{\text{A}}{\text{m}^2} \frac{\hbar}{2e}$, and the temperature rise in the sample is estimated to be on the order of 1 K, which is not high. If we further increase the electric field strength, then two main issues will arise. 1) On the experimental side, a strong laser may destroy the sample. This might happen for electric field strength above 10 MV/m when one uses a continuous wave laser. In this case, the spin current density is around $10^{10} \frac{\text{A}}{\text{m}^2} \frac{\hbar}{2e}$, which is quite large, while the temperature rise can be as high as 100 K. Note that the temperature rise can be mitigated with better thermal management. On the other hand, the sample may survive in an even stronger electric field if the pulsed laser is used. For example, with a femtosecond laser, the electric field can be as high as 100 MV/m, with a temperature rise of 10 K. 2) On the theoretical side, the perturbation theory used in the current work may fail when the electric field is too strong. The external electric field strength should be compared with the intrinsic interaction strength in the materials, which is usually on the order of $1 \text{ V}/\text{\AA} = 10^4 \text{ MV/m}$. From this point of view, the perturbation theory may work up to an electric field strength of 100 MV/m. Above this strength, the error from perturbative expansions may not be ignored and non-perturbation theories may be required.

In summary, with a pulsed laser, our theoretical picture may work up to an electric field strength

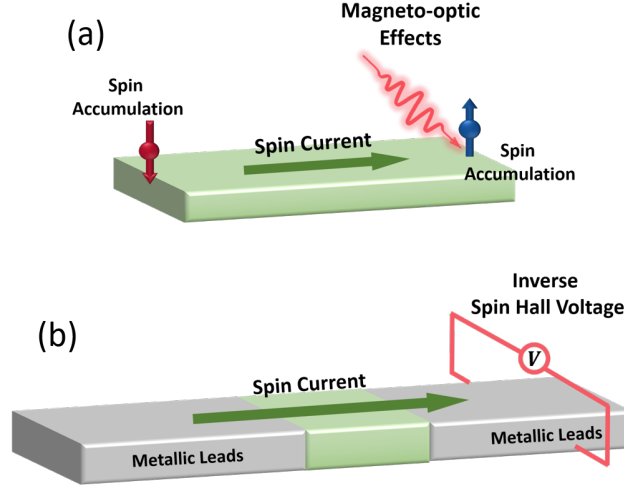


Figure S2: Approaches for detecting the spin current. (a) In a close circuit setup, there will be spin accumulations on both ends of the source material, which can be detected by magneto-optic effects. (b) In an open circuit setup, the spin current flows into metallic leads, and the inverse spin Hall voltage would be generated.

up to 100 MV/m, when the spin current density can be on the order of $10^{12} \frac{\text{A}}{\text{m}^2} \frac{\hbar}{2e}$. This is restricted by both experimental (sample damage) and theoretical (validity of perturbation theory) concerns. With a continuous wave laser, one may have to use an electric field strength below 10 MV/m to keep the temperature rise and sample damage manageable. At this field strength, the spin current density can be $10^{10} \frac{\text{A}}{\text{m}^2} \frac{\hbar}{2e}$ with the monolayer MoS₂ parameters.

5.3 Detection of the spin current

In the main text we discussed how the spin current can be detected. The schemes are illustrated in Fig. S2.

6 Computational benchmarks

In this section we provide computational benchmarks on our NLO spin/charge conductivity formula Eq. (S21).

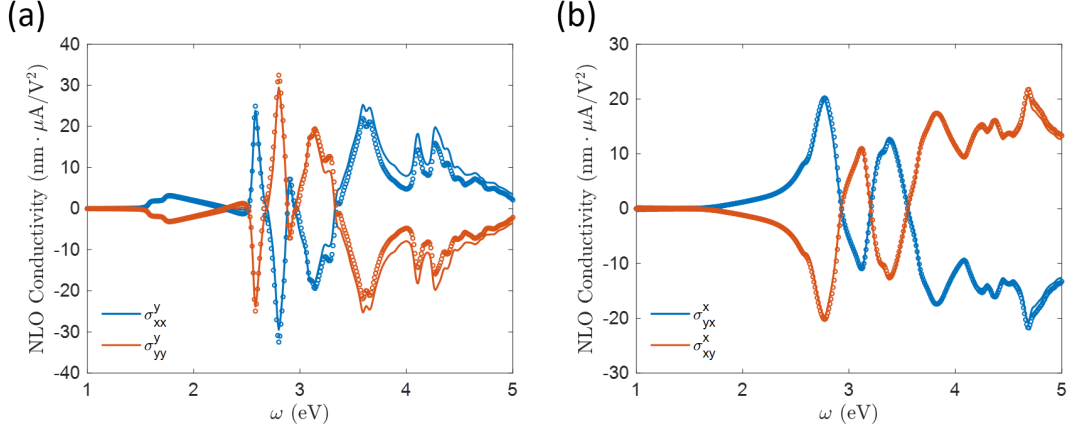


Figure S3: NLO charge conductivity of MoS₂ under LPL (a) and CPL (b). The solid lines are obtained with Eq. (S22), which uses the velocity gauge, while the dots are obtained with the well-known shift and injection current formulae Eqs. (S24, S28), which are in the length gauge. The two curves agree well with each other. There are minor discrepancies at high frequencies, and the reason is that only a finite number of conduction bands are used in the computation.

6.1 Numerical comparison between the velocity gauge and length gauge

- a. We compare the charge shift and injection conductivity from Eq. (S22), which is in velocity gauge, and from Eqs. (S24, S28), which is from length gauge. We take MoS₂ as an example and the results are shown in Fig. S3. One can see that the two curves agree well with each other. Note there are minor discrepancies at high frequency ($\omega > 3.5$ eV), this is because we only use a finite number of conduction bands in the calculation. The discrepancies should disappear when infinite number of conduction bands are involved.
- b. We reproduce the NLO charge conductivity for monolayer GeS, which was studied in Ref. [13]. Our results are shown in Fig. S4. One can see that it is in great agreement with Fig. 2 in Ref. [13].

6.2 NLO conductivity as a function of lifetime τ

The analysis in Sec. 3 demonstrates that under LPL, the charge (spin) currents of MoS₂ are shift (injection) like, while the charge (spin) currents of MBT are injection (shift) like (see also Table 2 in the main text). For shift (injection) like mechanism, the conductivity scales as τ^0 (τ^1). We have numerically tested the τ -dependence for MoS₂ and MBT. The results can be found in Figs. S5 and S6, respectively. The expected dependence on τ can be clearly observed.

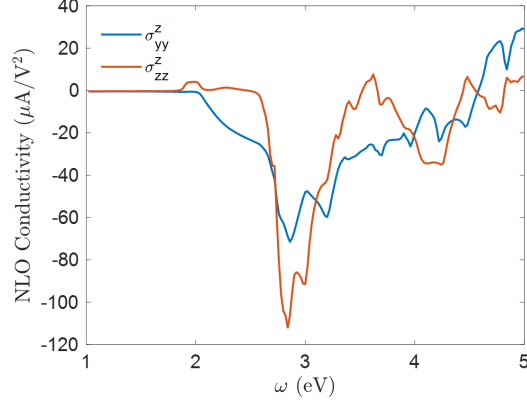


Figure S4: The NLO charge conductivity of monolayer GeS obtained with Eq. (S22), in agreement with results in Ref. [13] (Fig. 2 therein).

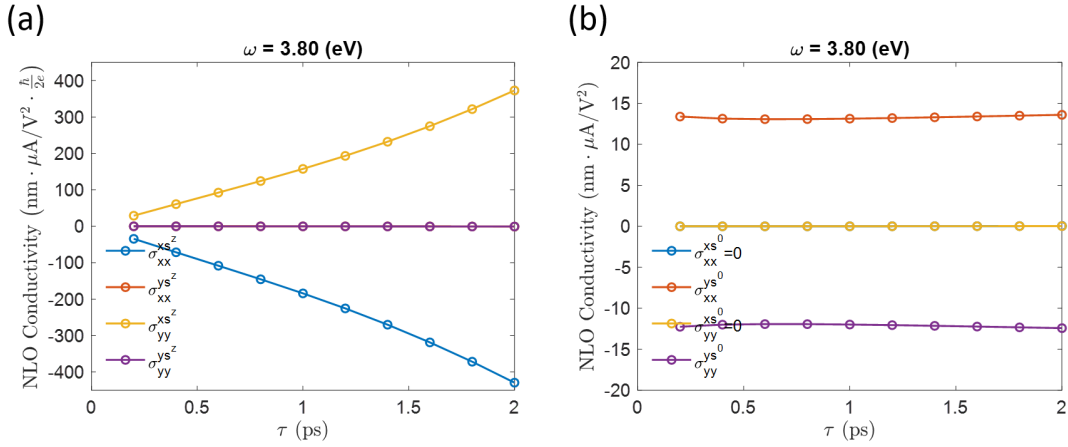


Figure S5: NLO spin (a) and charge (b) conductivity of MoS₂ under LPL as a function of carrier relaxation time τ . The spin conductivity is approximately linearly dependent on τ , while the charge conductivity remains a constant. Such behavior manifests that in a \mathcal{T} -symmetric system, the charge current comes from shift-like mechanism, while the spin current comes from injection-like mechanism under LPL. The conductivities are at $\omega = 3.8$ eV.

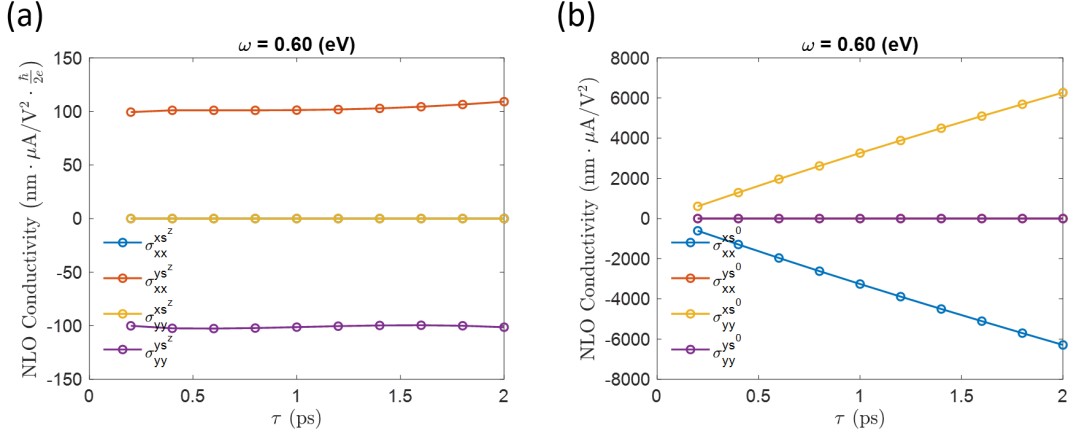


Figure S6: NLO spin (a) and charge (b) conductivity of MBT under LPL as a function of carrier relaxation time τ . The spin conductivity is approximately independent of τ , while the charge conductivity is approximately linearly dependent on τ . Such behavior manifests that in a \mathcal{PT} -symmetric system, the spin current comes from shift-like mechanism, while the charge current comes from the injection-like mechanism under LPL. The conductivities are at $\omega = 0.6$ eV.

6.3 NLO conductivity as a function of SOC strength

In the main text, we argued that in MBT, the NLO charge conductivity should increase with the SOC strength λ . This is computationally verified in Fig. S7.

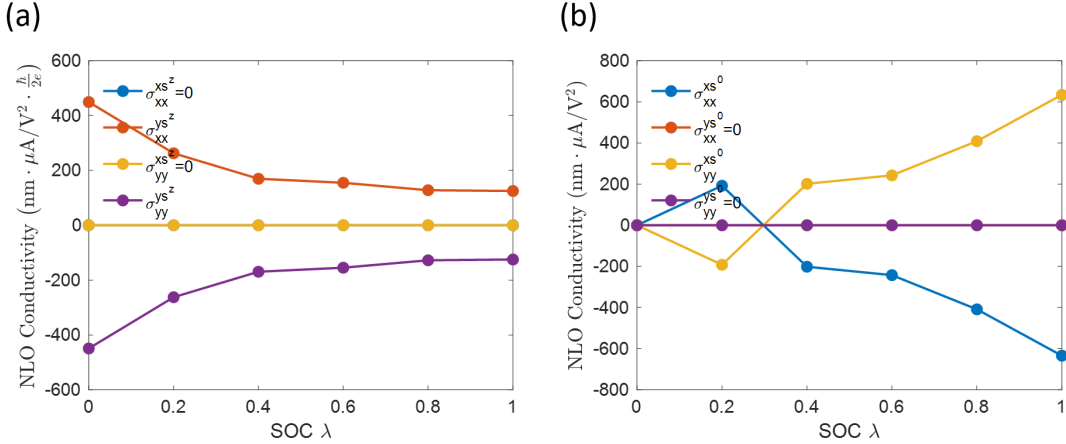


Figure S7: Peak values of NLO spin (a) and charge (b) conductivity of MBT as a function of SOC strength. As discussed in the main text, the spin conductivity is nonzero even when SOC is completely turned off ($\lambda = 0$), while the charge conductivity is zero when $\lambda = 0$ due to inversion-spin rotation symmetry and grows with λ . Note that SOC strongly modifies the band structure of MBT, thus the spin and charge conductivity have relatively more complicated dependence on λ , as compared that in the case of MoS_2 .

7 NLO spin current under circularly polarized light

In the main text, the NLO spin currents under LPL are presented. They correspond to the symmetric real part of Eq. (S21). In this section we show the spin current under CPL as in Figs. S8-S10, which correspond to the asymmetric imaginary part of Eq. (S21).

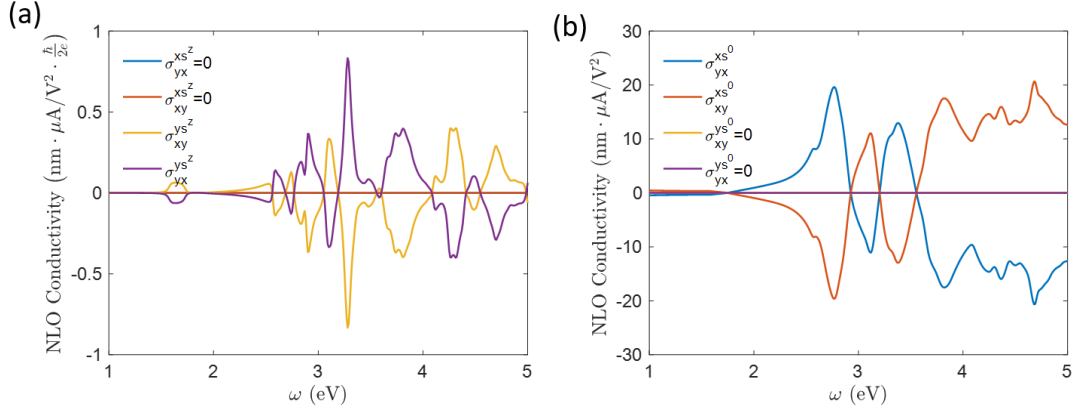


Figure S8: The NLO charge and spin- z conductivity of MoS₂ under CPL.

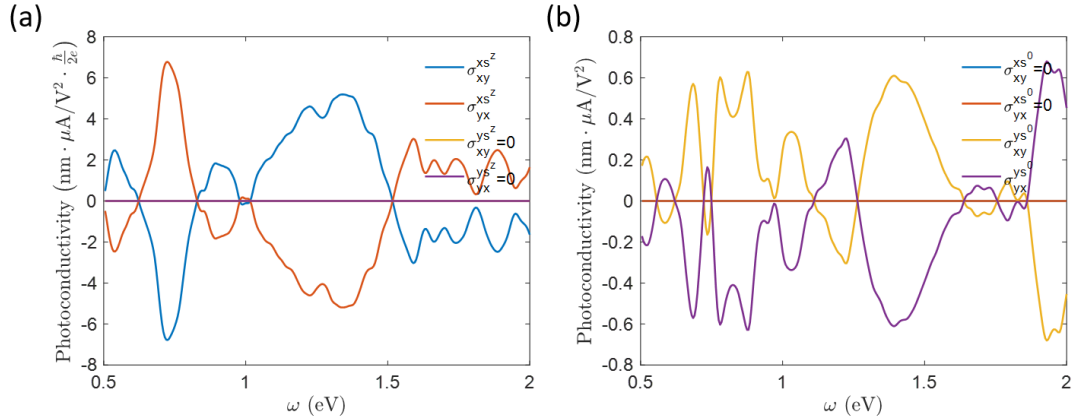


Figure S9: The NLO charge and spin- z conductivity of MnBi₂Te₄ under CPL.

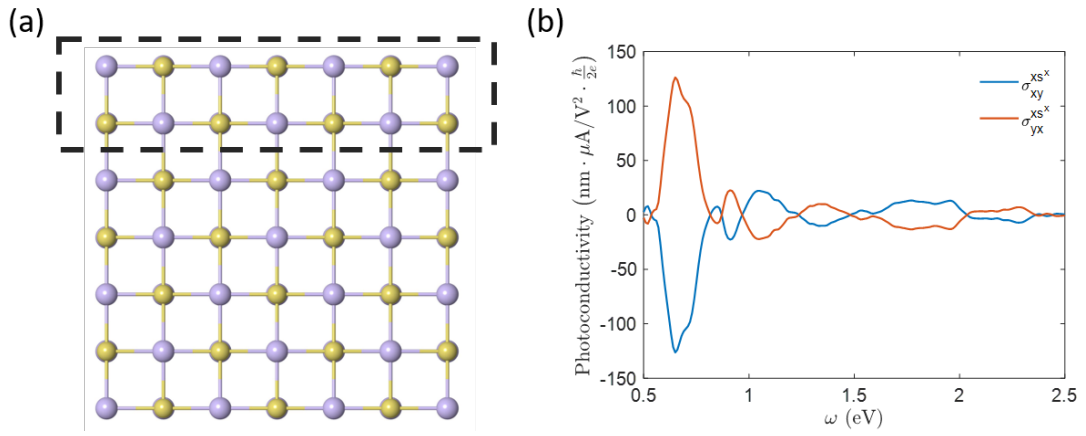


Figure S10: (a) Side view of SnTe. The dashed box indicate the out-most layer of SnTe. (b) The NLO spin conductivity of SnTe under CPL.

References

- [1] Kraut, W. & von Baltz, R. Anomalous bulk photovoltaic effect in ferroelectrics: a quadratic response theory. *Physical Review B* **19**, 1548 (1979).
- [2] von Baltz, R. & Kraut, W. Theory of the bulk photovoltaic effect in pure crystals. *Physical Review B* **23**, 5590 (1981).
- [3] Zhang, Y. *et al.* Photogalvanic effect in weyl semimetals from first principles. *Physical Review B* **97**, 241118 (2018).
- [4] Zhang, Y. *et al.* Switchable magnetic bulk photovoltaic effect in the two-dimensional magnet *cr* 3. *Nature communications* **10**, 1–7 (2019).
- [5] Sipe, J. & Shkrebtii, A. Second-order optical response in semiconductors. *Physical Review B* **61**, 5337 (2000).
- [6] Ventura, G., Passos, D., dos Santos, J. L., Lopes, J. V. P. & Peres, N. Gauge covariances and nonlinear optical responses. *Physical Review B* **96**, 035431 (2017).
- [7] Taghizadeh, A., Hipólito, F. & Pedersen, T. G. Linear and nonlinear optical response of crystals using length and velocity gauges: Effect of basis truncation. *Physical Review B* **96**, 195413 (2017).
- [8] Aversa, C. & Sipe, J. Nonlinear optical susceptibilities of semiconductors: Results with a length-gauge analysis. *Physical Review B* **52**, 14636 (1995).
- [9] Rashba, E. I. Spin currents in thermodynamic equilibrium: The challenge of discerning transport currents. *Physical Review B* **68**, 241315 (2003).
- [10] Sun, Q.-f., Xie, X. & Wang, J. Persistent spin current in nanodevices and definition of the spin current. *Physical Review B* **77**, 035327 (2008).
- [11] Shi, J., Zhang, P., Xiao, D. & Niu, Q. Proper definition of spin current in spin-orbit coupled systems. *Physical review letters* **96**, 076604 (2006).
- [12] Murakami, S. Quantum spin hall effect and enhanced magnetic response by spin-orbit coupling. *Physical Review Letters* **97**, 236805 (2006).
- [13] Rangel, T. *et al.* Large bulk photovoltaic effect and spontaneous polarization of single-layer monochalcogenides. *Physical review letters* **119**, 067402 (2017).

Reviewer #1:

Remarks to the Author:

Dear Editors,

The manuscript titled "Pure spin photocurrent in non-centrosymmetric crystals: bulk spin photovoltaic effect" shows that "nonlinear optical (NLO) effect can be used to generate pure spin currents" "if the system possesses additional mirror symmetry or inversion-mirror symmetry". Using a computational approach based on second order response, the authors compute a pure spin current for a few example materials to show the generation of a photo-spin current that significantly exceeds the photo charge current response.

The authors are motivated by "One of the core challenges of spintronics is the generation of the spin current, and particularly, a pure spin current without an accompanying charge current", which motivated by Ref 6, they believe "find applications in next generation energy efficient and ultrafast spintronics". Despite the somewhat extensive discussion, because of the rather extensive work in this field, I am not entirely convinced that the motivation for the work reaches the level of impact required for consideration in Nature Communications. Below I elaborate the reasons for my concern.

While it hasn't been called "injection current", the idea of generating spin currents through photoexcitation of semiconductors such as GaAs has been around for a while. This is clear from the fact that Fig 1a of PRL 96, 246601 (2006) has some at least superficial resemblance to Fig 1 of the current manuscript though the role of mirror symmetry is not as emphasized. As I understand it from the manuscript, the mirror symmetry leads to "a pure spin current can be realized, which is highly desirable for energy-efficient spintronics." This confuses me because as pointed out in Ref 1, a pure spin current does not guarantee lack of dissipation. Specifically, in this case, the optical excitation generates electron-hole pairs, which are highly energetically excited. I expect the relaxation of this excitation to lead to significant dissipation at some point. It seems that the authors are pointing out that TCIs such as SnSe, SnTe have an advantage relative to the GaAs example because of the double mirror symmetry, which should be emphasized more.

A more serious omission in terms of references in my view is PHYSICAL REVIEW B 102, 081402(R) (2020),

which has proposed an injection-based pure spin photocurrent in the quantum spin-Hall edge states of TMDs. The mechanism is quite similar to the one in the present work, though this is for a one dimensional edge in a two dimensional system.

Apart from motivational issues that I raised above, I have a few suggestions for the presentation of the formalism. The symmetry argument presented between lines 125-135, which is one of the main points of the manuscript seems to be a bit sloppy. This is because while Eq. 2, whose numerator is being discussed depends on off-diagonal matrix elements of the spin and velocity operators, they appear to be treated here as numbers. Also it would be good to clarify this.

Another technical aspect is the treatment/interpretation of the scattering time τ , which plays a somewhat important role. In the shift mechanism the time τ is a dephasing or scattering time for the electron-hole pair rather than the equilibration time suggested here. This has been recently clarified in PHYSICAL REVIEW B 101, 045201 (2020), where the second order response formula for the charge BVPE is shown to be equivalent to the dipole moment of electron hole pairs if τ is interpreted as a scattering time. In this sense, the injection mechanism is rather physically different and generates a current from a difference of velocities of the different excited charge carriers. This current survives for as long as the electrons/holes maintain their direction, leading to a different interpretation

for τ . I think these subtleties are lost in the second order response formula. Also the electron-hole pair interpretation provides a direct understanding of the symmetries in table 2. Shift currents occur when the excited pair has a dipole moment. Injection currents on the other hand are a result of unequal excitation of carriers of different velocities.

In summary, while I think the work is technically interesting, I am not sure I am convinced that the authors have clarified the motivation for this work that would lead to a high level of impact suggested for publication in Nature Communications.

Reviewer #2:

Remarks to the Author:

This is a timely work which shows theoretically how the nonlinear optical effect could be used to generate pure spin photocurrent in non-centrosymmetric crystals. These findings are illustrated on examples from three classes of materials, transition metal dichalcogenides (MoS₂), antiferromagnetic topological insulator (MnBi₂Te₄), and the surface state of the topological crystalline insulator (SnTe). Both the topic of generating (electrically, or optically) spin current and the considered materials classes are actively studied, so the findings of this manuscript have potential many implications. Specifically, as noted, for example, in Ref. 1, spin current provides an important element for spintronic applications as well as a tool to probe materials properties. Methods which would allow for a robust generation of pure spin current therefore have broad ramifications. The authors complement well their symmetry analysis and conductivity calculations by the materials-specific ab-initio calculations.

To provide a better context of this work and further explain its relevance, it would be helpful to give several explanations and clarify its underlying assumptions.

1) Adding a spin degree of freedom can generalize various photovoltaic effects that have been studied in common semiconductors and their junctions. See, for example, Appl. Phys. Lett. 79, 1558 (2001), Phys. Rev. Lett. 88, 066603 (2002), or related experiments, Nat. Commun. 4, 2068 (2013), which may be helpful to mention. Since the spin current is not conserved it may also be important to identify the position at which it is evaluated. Even in a simple p-n junction, illuminated by circularly-polarized light, a different voltage dependence of the spin and charge currents allows for a generation of pure spin current.

2) This non-conservation of the spin current has led to lots of debates about its definition, when the prediction of the spin Hall effect from Refs. 10, 11, was revisited 30 years later. It would help to clarify how the employed definition for spin current compares to the one from Phys. Rev. Lett. 96, 076604 (2006), which also recalls a cautionary work of Rashba [Phys. Rev. B 68, 241315(R) (2013)].

3) What are the employed assumptions for loss mechanisms of pure spin photocurrents? For example, in a simple situation analyzed in 1) in addition to the spin relaxation, the spin current can be lost through carrier recombination. This spin dynamics and spin-orbit coupling for electrons and holes are inequivalent.

4) Perhaps some clarification for the points above could be given by moving the p.15 comment about focusing only on intrinsic currents to an earlier place in the manuscript. Even in such intrinsic regime, how can one understand the corresponding time/length scales for the presence of spin photocurrents?

5) For an experimental detection of spin photocurrent, could one use spin extraction [predicted in Phys. Rev. Lett. and measured in Nat. Commun. noted above]?

6) References are not given in a uniform style. Some journal names are abbreviated, some not. Ref. 10 has typos and repeated authors, extra number appear in Ref. 27, 45, 67. Are Refs. 31, 40, 47 complete?

This manuscript describes an important opportunity to realize spin photocurrent in a wide range of materials. Following these clarifications, it will be easier to assess its suitability for a broad readership and a publication in Nature Communications.

Reply to Reviewers

Reviewer #1:

The manuscript titled "Pure spin photocurrent in non-centrosymmetric crystals: bulk spin photovoltaic effect" shows that "nonlinear optical (NLO) effect can be used to generate pure spin currents" "if the system possesses additional mirror symmetry or inversion-mirror symmetry". Using a computational approach based on second order response, the authors compute a pure spin current for a few example materials to show the generation of a photo-spin current that significantly exceeds the photo charge current response. The authors are motivated by "One of the core challenges of spintronics is the generation of the spin current, and particularly, a pure spin current without an accompanying charge current", which motivated by Ref 6, they believe "find applications in next generation energy efficient and ultrafast spintronics". Despite the somewhat extensive discussion, because of the rather extensive work in this field, I am not entirely convinced that the motivation for the work reaches the level of impact required for consideration in Nature Communications. Below I elaborate the reasons for my concern.

Reply: We thank the reviewer for these comments. Here we briefly list the motivations and novelties of our work:

- 1) We derived a unified theory of the generation of spin current under light illumination. Nonlinear optical (NLO) approaches have attracted great interest recently, as they can be non-contact (without e.g., electrochemical electrode deposition), non-destructive (does not induce unwanted impurities), and ultrafast (timescale on the order of picoseconds or even femtoseconds). Most previous theoretical and experimental efforts focus on how second-harmonics waves, charge current, etc. can be generated under light in different materials, while our theory points out the possibility of spin current generation with NLO effects. The bulk spin photovoltaic effect is the lowest-order NLO effect that can be used to generate dc spin current.
- 2) Our bulk spin photovoltaic effect is a universal and robust mechanism for spin current generation. Particularly, the only requirement to generate spin photocurrent is inversion symmetry breaking. There is no need for any special ingredients such as magnetic materials,

special device structures (quantum wells, junctions, etc.), the interference between two pulses, or specific light wavelength or polarization, which are required in many previous works. This would provide great flexibility in practice. Also, our theory applies to semiconductors, thus it may be readily integrated with existing semiconductor technologies, which is of significant importance as outlined by Albert Fert [*Rev. Mod. Phys.* **80**, 1517 (2008)]. These advantages, together with the flexibilities of optical approaches (dynamic spatial addressability, tunable intensity, wavelength, polarization, etc.), provide a large playground to be explored. Many spintronic applications (e.g., spin injection into semiconductors, spin FET, spin battery, and spin-dependent energy-harvesting [*Commun. Mater.* **1**, 24 (2020)]) may be realized in an easier fashion with such an optical approach. For example, spin current can be generated in bulk GaAs under sunshine, as we do not need circularly polarized light.

- 3) We explicitly reveal that the symmetry condition for hosting *pure* spin current is to possess mirror symmetry \mathcal{M} , inversion-mirror symmetry \mathcal{PM} , or inversion-spin rotation symmetry \mathcal{PS} . This provides a simple but effective guideline for pure spin current generation under light. Particularly, we studied the surface states of a topological material SnTe, whose double mirror symmetry indicates that the charge current all vanishes, while the spin current can survive on the surfaces. These results are useful not only for generating pure spin currents, but also for the probe of surface states properties of topological materials.
- 4) We also made several other theoretical advances. For example, we clarify and compare the mechanism (shift and/or injection mechanisms) for spin current generation under different symmetry conditions (\mathcal{T} , \mathcal{PT} , etc.) and different light polarizations (linear and circularly polarized light). This illuminates the microscopic mechanisms for spin current generation. We also clarified the important role of the spin-orbit coupling (SOC). On one hand, it can lead to a spin texture in non-magnetic materials, which is necessary for spin current generation. But on the other hand, in many cases SOC breaks the inversion-spin rotation symmetry \mathcal{PS} , hindering the realization of pure spin current.
- 5) Besides the above advances on the physical mechanism for spin current generation, we also computationally studied the bulk spin photovoltaic effect with several different material classes that are attracting great interest recently, which may guide the potential applications for these materials. It also helps the development of next-generation devices with next-generation materials.

We have revised several parts of our manuscript to strengthen the motivation and novelties of our work, including,

- On page 4, we added, “Here we would like to emphasize that the only general requirement for our NLO spin current is \mathcal{P} breaking, and there is no need for any special ingredients such as magnetic materials, special device structures (quantum wells, junctions, etc.), the interference between two pulses, or specific light wavelength or polarizations. This would provide great convenience in practice and can be readily integrated with existing semiconductor technologies. These flexibilities, together with the flexibilities of optical approaches (dynamic spatial addressability, tunable intensity, wavelength, polarization, etc.), provide a large playground to be explored. Many applications that are not envisaged before may become possible.”
- On page 4, we added, “Particularly, when double mirror symmetries, or inversion-spin rotation symmetry \mathcal{PS} are present, the charge current would all vanish (even in the transverse directions), while the spin current can survive. These results are useful not only for generating pure spin currents, but also for material characterization.”
- On page 4, we added, “We also clarify the mechanisms (shift and/or injection like) for spin current generation under different symmetry conditions (\mathcal{P} and \mathcal{T}) and under light with different polarization (LPL and CPL).”
- On page 4, we added, “....., where the “voltaic” is defined as $V_{\uparrow\downarrow} \equiv \frac{\mu_{\uparrow} - \mu_{\downarrow}}{-e}$, the difference in chemical potential (μ) between spin-up (\uparrow) and spin-down (\downarrow) electrons, unlike the BPVE voltage that may be defined as $U \equiv \frac{\mu_{\uparrow} + \mu_{\downarrow}}{-2e}$. Similar to the BPVE voltage U , $V_{\uparrow\downarrow}$ will not be limited by the bandgap of the material, and the currents will not be limited by the Shockley–Queisser limit.”
- On page 8, we added, “..... The results suggest that our mechanism for spin current generation is general and robust in these distinct systems.”
- On page 13, we added, “These results suggest that while SOC can enable spin current in non-magnetic materials such as MoS₂, it would, on the other hand, hinder the generation of pure spin current in some cases. Also, SOC should be treated rigorously when studying both the spin current and the charge current.”

- On page 17, we added, “The predicted BSPV and light-induced pure spin current do not have special requirements except for inversion symmetry breaking, and can be readily integrated with existing semiconductor technologies.”

Below is our point-to-point response to the reviewer’s comments.

1) While it hasn't been called "injection current", the idea of generating spin currents through photoexcitation of semiconductors such as GaAs has been around for a while. This is clear from the fact that Fig 1a of PRL 96, 246601 (2006) has some at least superficial resemblance to Fig 1 of the current manuscript though the role of mirror symmetry is not as emphasized.

Reply: We thank the reviewer for pointing out this interesting work from A. L. Smirl and H. M. van Driel groups. Actually, we have cited a similar but earlier work from the same groups (Ref. 18, [*PRL* **90**, 136603 (2003)]). These works, together with some other relevant works focusing on the charge current, e.g., [*PRL* **76**, 1703 (1996), *PRL* **78**, 306 (1997), etc.], employed the two-color quantum interference control (QUIC). As we will elaborate on below, this mechanism is fundamentally distinct from that in our work, although it is also an optical approach.

1) A prominent difference is that the QUIC requires two beams with frequencies ω and 2ω simultaneously. And the spin/charge current generation is dependent on the relative phases of these two beams (quantum interference). On the other hand, our approach requires only one beam and does not require stringent phase-matching conditions, which is more convenient in practice.

2) QUIC is a (at least) third-order effect. The charge and spin current originate in the interference between the 2ω beam and the ω beam, which is $\propto E(-2\omega)E(\omega)E(\omega)$, where $E(\omega)$ is the Fourier component of the electric field at frequency ω . Besides, the optical excitation from the ω laser beam is a two-photon process and should be a fourth-order effect $\propto E(-\omega)E(+\omega)E(-\omega)E(\omega)$. These facts are evident in two theoretical papers [*PRL* **76**, 1703 (1996), *PRL* **85**, 5432 (2000)]. As a higher-order effect, QUIC would generally be less efficient and smaller in magnitude than the second-order effect in our work.

3) Specific to spin current generation, QUIC requires a narrow frequency window “so that there are no transitions from the (spin) split-off band” [*PRL* **85**, 5432 (2000)]. Such a window is about

0.3 eV in GaAs. On the other hand, our mechanism is applicable for a wide frequency window, as shown in Figures 2-4 in the main text.

On the other hand, QUIC has its own advantages. For example, it does not require inversion symmetry breaking (as it being a third-order nonlinear optical process). Besides, the relative phase between the two beams could provide another degree of freedom to control the spin and charge currents. We agree with the reviewer that the approach for obtaining *pure* spin current in these works is similar to that in our work – once we have counter-propagating electrons with opposite (or at least different) spin polarization, then a pure spin current arises. Actually, this approach is also used in e.g., spin Hall effect [*PRL* **95**, 226801 (2005)]. However, for spin current generation QUIC is a distinct mechanism from the bulk spin photovoltaic effect proposed in our work, as we described above.

2) As I understand it from the manuscript, the mirror symmetry leads to "a pure spin current can be realized, which is highly desirable for energy-efficient spintronics." This confuses me because as pointed out in Ref 1, a pure spin current does not guarantee lack of dissipation. Specifically, in this case, the optical excitation generates electron-hole pairs, which are highly energetically excited. I expect the relaxation of this excitation to lead to significant dissipation at some point.

Reply: We thank the reviewer for pointing out this misleading statement. We did not intend to claim that the generation of spin current, or the flow of spin current, is free of energy dissipation. We intended to express that the pure spin current may be more favorable than a non-pure spin current (mixed with charge currents) for spintronic applications. This is because an accompanying charge current may lead to undesired side effects such as charge accumulation and additional dissipations. We have removed the “energy-efficient” and revised this statement as

“a pure spin current can be realized, which does not carry charge degree of freedom and is more favorable than a non-pure spin current for many spintronics applications.”

We have also revised statements about energy efficiency in several other places in the main text to avoid similar misunderstandings.

Next, we show that for spin current generation, the temperature rise due to the energy dissipation is generally not significant. Here we take monolayer MoS₂ as an example. For the bulk spin photovoltaic effect studied in this work, the main energy consumption is the photon absorption due to interband transitions (electron-hole pair generation), and the absorbance is $A = 1 - \exp\left[-\frac{\omega}{c\epsilon_0}\epsilon^i(\omega)d\right] \approx \frac{\sigma^r(\omega)}{c\epsilon_0}d$, where ϵ_0 is the vacuum permittivity, ϵ^i is the imaginary part of the dielectric function, σ^r is the real part of the optical conductivity (one has $\epsilon(\omega) = \epsilon_0 + \frac{i\sigma(\omega)}{\omega}$). d is the thickness of the material, which is taken as 0.6 nm for MoS₂. The energy consumption rate per unit area is

$$\begin{aligned} P &= AI & (R1) \\ &= \frac{\sigma^r(\omega)}{c\epsilon_0}d \cdot \frac{\epsilon_0 c}{2}E^2 \\ &= \frac{\sigma^r(\omega)d}{2}E^2 \end{aligned}$$

where $I = \frac{\epsilon_0 c}{2}E^2$ is the intensity of the light. From our *ab initio* calculations, at $\omega = 3$ eV one has $\sigma^r(\omega) = 4 \times 10^5 \Omega/\text{m}$. In the main text, we showed that light with electric field strength on the order of $E = 100$ V/m would be able to generate a detectable spin current. With this field strength, the energy consumption power is only $P = 1.2 \times 10^{-4}$ W/cm², which is rather small. Here we calculate the temperature rise under an electric field of $E = 1$ MV/m, which is much stronger, but readily available with laser technology. Under this field strength, one has $P = 1.2 \times 10^4$ W/cm². Assume that MoS₂ is put on a substrate with thermal conductivity κ and thickness l_{subs} . If a continuous wave (CW) light is used, then the steady-state temperature rise can be roughly estimated from

$$\Delta T_{\text{CW}} = \frac{P}{\kappa}l_{\text{subs}} \quad (R2)$$

Assuming that $l_{\text{subs}} = 1 \mu\text{m}$ and $\kappa = 100 \text{ W} \cdot \text{m}^{-1} \cdot \text{K}^{-1}$, then $\Delta T_{\text{CW}} \approx 1.2$ K, which is not significant. On the other hand, if a pulse laser is used, then the temperature rise can be estimated from

$$\Delta T_{\text{pulsed}} = \frac{\tau_{\text{pulse}}PS}{k_B} \quad (R3)$$

Where S is the area of a unit-cell, k_B is the Boltzmann constant, while τ_{pulse} is the duration of the pulse, and is taken as 1 ps here. One can find that $\Delta T_{\text{pulsed}} \approx 0.7$ K, which is not significant as well.

We would like to note that, not all energies absorbed by the materials go to the phonon (lattice) system (non-radiative recombination). They could recombine and re-emit photons. Therefore, the temperature rise in the ion system may be even lower than ΔT_{CW} and ΔT_{pulsed} estimated above.

We have added the discussions above in the Supplementary Materials.

3) It seems that the authors are pointing out that TCIs such as SnSe, SnTe have an advantage relative to the GaAs example because of the double mirror symmetry, which should be emphasized more.

Reply: We thank the reviewer for this helpful suggestion. We have emphasized more the unique role of double mirror symmetry for generating pure spin current. We have also emphasized more on the inversion-spin rotation symmetry \mathcal{PS} .

On page 4, we added “Particularly, when double mirror symmetries, or inversion-spin rotation symmetry \mathcal{PS} are present, the charge current would all vanish (even in the transverse directions), while the spin current can survive. These results are useful not only for generating pure spin currents, but also for material characterization.”

On page 15, we added “There may be other systems that possess double mirror symmetries, such as monolayer FeSe⁷³. They may also be good candidates for pure spin current generation.”

We have also explicitly discussed the role of double mirror symmetries in several other places in the manuscript, particularly in the *Surface States of Topological Materials* section.

4) A more serious omission in terms of references in my view is PHYSICAL REVIEW B 102, 081402(R) (2020), which has proposed an injection-based pure spin photocurrent in the quantum spin-Hall edge states of TMDs. The mechanism is quite similar to the one in the present work, though this is for a one-dimensional edge in a two-dimensional system.

Reply: We thank the reviewer for pointing out this paper [*PRB* **102**, 081402(R) (2020)]. This work uses patterned graphene nanoribbons with antiferromagnetic (AFM) edge states. Actually, we were aware of the paper when preparing our manuscript. But we decided not to cite this paper because:

1) First, it requires exquisite designing and fabricating processes. As indicated in the paper, the graphene nanoribbon needs to be patterned with triangle anti-dots, and it needs to “have opposite band structures and anti-symmetrical spin density for the two leads in their ground state”. These conditions are stringent. For example, the edge states are not necessarily AFM if a different patterning structure is used.

2) Secondly, a more serious problem is that the “pure spin current” “with spatial inversion symmetry” claimed in this paper may be *erroneous*. As indicated in this paper, the carbon atoms on the edges of the anti-dots have AFM spin coupling. Therefore, the system actually does *not* have spatial inversion symmetry, when the magnetism is taken into consideration. Hence, both the nonlinear spin current and the nonlinear charge current are allowed, according to our symmetry analysis. This is vividly illustrated with AFM bilayer MnBi_2Te_4 in our work. The atomic structure of AFM bilayer MnBi_2Te_4 also has inversion symmetry, but the anti-ferromagnetic moments on the upper and lower layers break the inversion symmetry. As shown in Figure 3 in our manuscript, if SOC is not taken into consideration, then the total charge current would be zero, consistent with the claim in [*PRB* **102**, 081402(R) (2020)]. However, if we consider SOC, which transfers the inversion asymmetry in spin degree of freedom to the orbital degree of freedom, then the charge current would be non-zero as well. In [*PRB* **102**, 081402(R) (2020)], the “pure spin current” comes from the fact that SOC is ignored, and that the spin up and down states are treated separately. If SOC is rigorously considered, then the charge current should appear.

On the other hand, in the present work, we clarify that mirror symmetry can lead to pure spin current (with possible charge current in the transverse direction). Also, in some cases when double mirror symmetries exist, the charge current can be totally forbidden (absent even in the transverse directions). Besides, we propose that inversion-spin rotation symmetry \mathcal{PS} can guarantee pure spin current without any charge current as well, which may be realized in e.g.,

skyrmion systems, or magnetic materials with canted or all-in-all-out magnetic configurations, etc. This is based on careful symmetry analysis and is robust even under strong SOC effects.

Finally, we would like to remark that [PRB 102, 081402(R) (2020)] is not dealing with “the quantum spin-Hall edge states of TMDs”, but edge states of graphene nanoribbons. However, we could not find a work that studies “injection-based pure spin photocurrent in the quantum spin-Hall edge states of TMDs”. Thus, we focused on [PRB 102, 081402(R) (2020)]. Two other works [PRB 100, 195410 (2019)] and [PRL 115, 166804 (2015)] study the spin currents in 2H TMDs (which are not quantum spin Hall insulators). But they are also different from our work. Specifically, [PRB 100, 195410 (2019)] requires the proximity effect with magnetic material, and the authors did not claim “pure” spin current (actually it should not be pure spin current). On the other hand, [PRL 115, 166804 (2015)] requires the 2H-WSe₂/2H-MoSe₂ heterostructure and two spatially varying laser beams applied simultaneously.

5) Apart from motivational issues that I raised above, I have a few suggestions for the presentation of the formalism. The symmetry argument presented between lines 125-135, which is one of the main points of the manuscript seems to be a bit sloppy. This is because while Eq. 2, whose numerator is being discussed depends on off-diagonal matrix elements of the spin and velocity operators, they appear to be treated here as numbers. Also, it would be good to clarify this.

Reply: We thank the reviewer for these helpful comments. We have cleared up the confusions and explicitly added the matrix indices, and revised these arguments as

“Next, we consider symmetry constraints on the conductivity tensor. First, we note that the numerators are composed of terms with format $N_{mnl}^{iabc} = j_{mn}^{a,s^i} v_{nl}^b v_{lm}^c$ with $i \neq 0$ for spin current and use $N_{mnl}^{0abc} = v_{mn}^a v_{nl}^b v_{lm}^c$ for charge current. Under spatial inversion operation \mathcal{P} , one has $\mathcal{P}v_{mn}^a(\mathbf{k}) = -v_{mn}^a(-\mathbf{k})$, $\mathcal{P}s_{mn}^i(\mathbf{k}) = s_{mn}^i(-\mathbf{k})$, and $\mathcal{P}j_{mn}^{a,s^i}(\mathbf{k}) = -j_{mn}^{a,s^i}(\mathbf{k})$. Thus $\mathcal{P}N_{mnl}^{iabc}(\mathbf{k}) = -N_{mnl}^{iabc}(-\mathbf{k})$. On the other hand, the denominator is invariant under \mathcal{P} , thus all components (including charge and spin) of σ_{bc}^{a,s^i} should vanish after a summation over $\pm\mathbf{k}$ in \mathcal{P} -conserved systems. Therefore, the inversion symmetry \mathcal{P} has to be broken to give nonvanishing σ_{bc}^{a,s^i} . Regarding time-reversal operation \mathcal{T} , one has $\mathcal{T}v_{mn}^a(\mathbf{k}) = -v_{mn}^{a*}(-\mathbf{k})$, $\mathcal{T}s_{mn}^i(\mathbf{k}) = -s_{mn}^{i*}(-\mathbf{k})$

(Here \cdot^* indicates complex conjugate of \cdot). For charge current, one has $\mathcal{T}N_{mnl}^{0abc}(\mathbf{k}) = -N_{mnl}^{0abc*}(-\mathbf{k})$. Thus, the real and imaginary part of N_{mnl}^{0abc} are odd and even under \mathcal{T} , respectively. The imaginary part of $N^{0abc}(\mathbf{k})$ contributes to the total charge conductivity after the summation over $\pm\mathbf{k}$ in a \mathcal{T} -conserved system. Similarly, for spin- i current ($i \neq 0$), one has $\mathcal{T}N_{mnl}^{iabc}(\mathbf{k}) = N_{mnl}^{iabc*}(-\mathbf{k})$, thus it is the real part of $N^{iabc}(\mathbf{k})$ that contributes to the total spin conductivity.”

We have also added the matrix indices in Table I and several other places in the main text.

6) Another technical aspect is the treatment/interpretation of the scattering time τ , which plays a somewhat important role. In the shift mechanism the time τ is a dephasing or scattering time for the electron-hole pair rather than the equilibration time suggested here. This has been recently clarified in PHYSICAL REVIEW B 101, 045201 (2020), where the second order response formula for the charge BVPE is shown to be equivalent to the dipole moment of electron hole pairs if τ is interpreted as a scattering time. In this sense, the injection mechanism is rather physically different and generates a current from a difference of velocities of the different excited charge carriers. This current survives for as long as the electrons/holes maintain their direction, leading to a different interpretation for τ . I think these subtleties are lost in the second order response formula. Also the electron-hole pair interpretation provides a direct understanding of the symmetries in table 2. Shift currents occur when the excited pair has a dipole moment. Injection currents on the other hand are a result of unequal excitation of carriers of different velocities.

Reply: We thank the reviewer for these insightful comments. We agree that the scattering time τ is rather important. Here we would like to use the charge current as an example to illustrate the role of τ , which is more straightforward, while a similar analysis applies to spin current.

The photocurrent is $j^a = \sigma_{bc}^a E^b E^c$. First, we note that a charge current j is odd under time-reversal symmetry \mathcal{T} , while electric field E is even under \mathcal{T} . If the system is non-magnetic, and we use linearly polarized light (LPL), then it seems that \mathcal{T} should be preserved. In this case, it seems that σ_{bc}^a should be zero, because the j^a is odd under \mathcal{T} , while $E^b E^c$ is even. However, in practice, the nonlinear photocurrent does exist, which is the shift current. Actually, \mathcal{T} is broken

by dissipation, which is characterized by τ . Therefore, the dissipation τ is indispensable for the shift current, although the shift current conductivity σ_{bc}^a is independent of τ .

This point can also be verified mathematically. The nonlinear photoconductivity is,

$$\sigma_{bc}^a(0; \omega, -\omega) = -\frac{e^2}{\hbar^2 \omega^2} \int \frac{d\mathbf{k}}{(2\pi)^3} \sum_{mnl} \frac{f_{lm} v_{lm}^b}{\omega_{ml} - \omega + i/\tau} \left(\frac{v_{mn}^a v_{nl}^c}{\omega_{mn} + i/\tau} - \frac{v_{mn}^c v_{ml}^a}{\omega_{nl} + i/\tau} \right) \quad (\text{R4})$$

Under time-reversal \mathcal{T} operation, one has $\mathcal{T}v_{mn}(\mathbf{k}) = -v_{mn}^*(-\mathbf{k})$, where $*$ indicates the complex conjugate. Thus, the numerator in Eq. (R4), $N_{mnl} = v_{mn}v_{nl}v_{lm}$, would behave as $\mathcal{T}N_{mnl}(\mathbf{k}) = -N_{mnl}^*(-\mathbf{k})$, while the denominator is invariant under \mathcal{T} . After the summation over $\pm\mathbf{k}$, the numerator becomes purely imaginary. No dissipation indicates $\tau = \infty$ and $\frac{i}{\tau} = 0$. In this case, the denominator would be purely real. Therefore, under LPL the whole formula is purely imaginary, and cannot contribute a static current, which should be a real number. Therefore, from a mathematical point of view, a finite τ is indispensable.

These arguments agree with those in [PRB **101**, 045201 (2020)]. That is, τ describes some processes that lead to dissipation, and thus 1) absorb energy from light and 2) break time-reversal symmetry. In [PRB **101**, 045201 (2020)] τ was suggested to be the scattering time with phonon. But in our view, it could also be the scattering with impurities, etc. Phenomenologically, one should have $\frac{1}{\tau} = \frac{1}{\tau_{\text{phonon}}} + \frac{1}{\tau_{\text{impurities}}} + \dots$; that is, τ incorporate contributions from all sources of dissipations. For convenience, we adopted the constant relaxation time approximation and used a constant τ for all modes (band index n and wavevector k). But in reality, τ should be mode-dependent (e.g., different for electrons and holes) and incorporates the subtleties described above. More discussions on τ can be found in our reply to the 3rd comment of Reviewer #2 (on page 16-17 of this document).

We have added the discussions about the role of τ on page 7 of the main text,

“We would like to briefly discuss the carrier lifetime τ . It has a rather important role. Here we use the charge current as an example to illustrate the role of τ , which is more straightforward. Similar analysis applies to spin current. The photocurrent is $j^a = \sigma_{bc}^a E^b E^c$. First, we note that a charge current j is odd under time-reversal symmetry \mathcal{T} , while electric field component E is even under \mathcal{T} . If the system is non-magnetic, and we use linearly polarized light (LPL), then it seems

that \mathcal{T} should be preserved. In this case, it seems that σ_{bc}^a should be zero, because the j^a is odd under \mathcal{T} , while $E^b E^c$ is even. However, in practice, the nonlinear photocurrent does exist, which is the shift current. Actually, \mathcal{T} is broken by dissipation, which is characterized by τ . Therefore, the dissipation τ is indispensable for the shift current, although the shift current conductivity σ_{bc}^a is independent of τ .”

Regarding the physical mechanisms of shift and injection currents, they are more evident when we use the length gauge. In the Supplementary Materials, we showed that the velocity gauge and the length gauge are equivalent. In the length gauge, one has (Eqs. (S27, S28) in the SM, Section 2),

$$\begin{aligned}\zeta_{aa}^c(0; \omega, -\omega) &= -\frac{i\pi e^3}{2\hbar^2} \int \frac{d\mathbf{k}}{(2\pi)^3} \sum_{n,m} f_{nm} R_{nm;c}^a |r_{mn}^a|^2 \delta(\omega_{mn} - \omega) \\ \eta_{ab}^c(0; \omega, -\omega) &= \frac{\pi\tau e^3}{2\hbar^2} \int \frac{d\mathbf{k}}{(2\pi)^3} \sum_{n,m} f_{nm} \Delta_{mn}^c [r_{mn}^a, r_{nm}^b] \delta(\omega_{mn} - \omega)\end{aligned}\tag{R5}$$

Here ζ_{aa}^c and η_{ab}^c are the shift and injection current conductivity, respectively. $|r_{mn}^a|^2$ and $[r_{mn}^a, r_{nm}^b]$ are proportional to the interband transition rate (electron-hole pair generation rate) under linearly and circularly polarized light, respectively. $R_{mn;c}^a = \frac{\partial \phi_{nm}}{\partial k^a} + \xi_{nn}^a - \xi_{mm}^a$ can be regarded as the dipole moment of the electron-hole pair, with ξ_{nn}^a as the center of the lattice-periodic wavefunction of band n (for details see SM). $\Delta_{mn}^c = v_{mm}^c - v_{nn}^c$ is the velocity difference between the conduction and valence bands. These length gauge formulae are reminiscent of the Fermi’s golden rule. The physical meanings of the shift and injection currents are thus evident, which agrees well with the interpretations suggested by the reviewer. Hence, we also added these discussions in the last paragraph on page 15 of the main text:

“The shift current mechanism comes from the fact that the wavefunction center of the electrons and holes are different, leading to an electric dipole upon electron-hole pair generation. On the other hand, the injection mechanism comes from the fact that the electrons and holes have different velocities, leading to a net current. These facts are more evident if we transform Eq. (2) into the length gauge, as shown in the SM.”

The detailed discussions above have been added in the Supplementary Materials.

In summary, while I think the work is technically interesting, I am not sure I am convinced that the authors have clarified the motivation for this work that would lead to a high level of impact suggested for publication in Nature Communications.

Reply: We thank the reviewer for these comments. We hope that we have appropriately addressed the concerns of the reviewer. We believe that our work is of broad impact for publication in Nature Communications.

Reviewer #2:

This is a timely work which shows theoretically how the nonlinear optical effect could be used to generate pure spin photocurrent in non-centrosymmetric crystals. These findings are illustrated on examples from three classes of materials, transition metal dichalcogenides (MoS₂), antiferromagnetic topological insulator (MnBi₂Te₄), and the surface state of the topological crystalline insulator (SnTe). Both the topic of generating (electrically, or optically) spin current and the considered materials classes are actively studied, so the findings of this manuscript have potential many implications. Specifically, as noted, for example, in Ref. 1, spin current provides an important element for spintronic applications as well as a tool to probe materials properties. Methods which would allow for a robust generation of pure spin current therefore have broad ramifications. The authors complement well their symmetry analysis and conductivity calculations by the materials-specific ab-initio calculations.

Reply: We appreciate these positive and encouraging comments from the reviewer.

To provide a better context of this work and further explain its relevance, it would be helpful to give several explanations and clarify its underlying assumptions.

1) Adding a spin degree of freedom can generalize various photovoltaic effects that have been studied in common semiconductors and their junctions. See, for example, Appl. Phys. Lett. 79, 1558 (2001), Phys. Rev. Lett. 88, 066603 (2002), or related experiments, Nat. Comm. 4, 2068

(2013), which may be helpful to mention. Since the spin current is not conserved it may also be important to identify the position at which it is evaluated. Even in a simple p-n junction, illuminated by circularly polarized light, a different voltage dependence of the spin and charge currents allows for a generation of pure spin current.

Reply: We thank the reviewer for these helpful comments and references. We have carefully read these interesting works. They are based on mechanisms reminiscent of the p-n junctions used in solar cells. This is distinct from our work, which is realizable in homogeneous materials and does not require hetero-junctions. Also, we do not need circularly polarized light. We have cited these works in the first paragraph on page 2 of the revised manuscript:

“Also, a spin current can be generated with a mechanism reminiscent of the p-n junction in solar cells^{25–27}.”

2) This non-conservation of the spin current has led to lots of debates about its definition, when the prediction of the spin Hall effect from Refs. 10, 11, was revisited 30 years later. It would help to clarify how the employed definition for spin current compares to the one from Phys Rev. Lett. 96, 076604 (2006), which also recalls a cautionary work of Rashba [Phys. Rev. B 68, 241315(R) (2013)].

Reply: We thank the reviewer for these insightful comments. Indeed, the definition of spin current is still under some debate. The conventional definition $\hat{j}_1 = \frac{1}{2}(\hat{v}\hat{s} + \hat{s}\hat{v})$ is indeed not well defined, although it is convenient, physically appealing, and extensively employed in many works until today. When SOC is taken into account, spin component is not a good quantum number, and this spin current is not conserved. Also, as suggested in Rashba’s work [PRB 68, 241315(R) (2003)], this definition would lead to a non-zero spin current even if an inversion asymmetric insulator is in equilibrium (no electric field, light, etc.). There are lots of debates, and there are also works claiming that we do not need to modify this definition [e.g., PRB 77, 035327 (2008)].

The definition in [PRL 96, 076604 (2006)], which is $\hat{j}_2 = \frac{d(\hat{r}\hat{s})}{dt}$, can be conserved in some systems. However, it requires that “spin generation in the bulk is absent due to symmetry

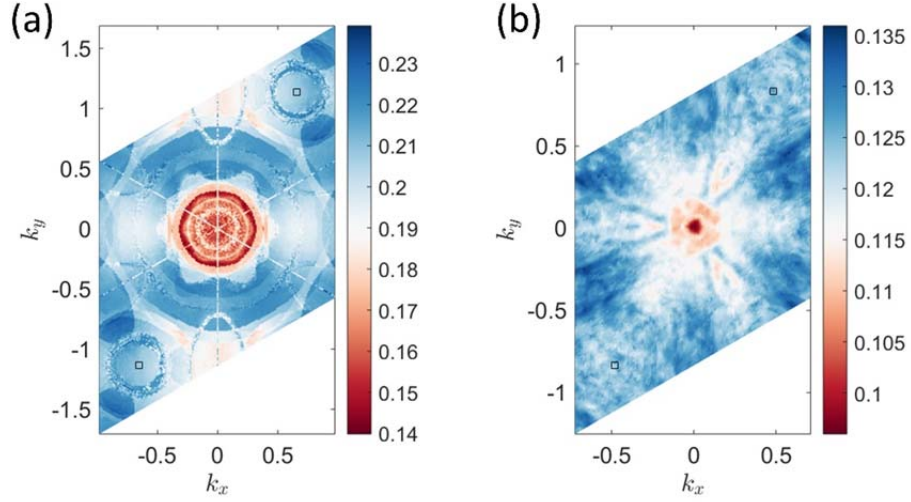


Figure R1 $\alpha_z \equiv \frac{\|[\hat{H}, \hat{s}^z]\|}{\|\hat{H}\| \cdot \|\hat{s}^z\|}$ for (a) MoS₂ and (b) MnBi₂Te₄.

reasons”. In other words, it requires the bulk integration $\frac{1}{V} \int dV \mathfrak{T}(r) = 0$, where $\mathfrak{T}(r)$ is the torque density on the spins. However, this is not true under external light, which is necessary for our work. An intuitive picture is, under a circularly polarized light, the angular momentum of the photons can be transferred into the electron system, which obviously leads to $\frac{1}{V} \int dV \mathfrak{T}(r) \neq 0$. Therefore, the definition of $\hat{j}_2 = \frac{d(\hat{r}\hat{s})}{dt}$ is also not correct if the system is under light illumination. Particularly, under strong light, the non-conservation of $\hat{j}_2 = \frac{d(\hat{r}\hat{s})}{dt}$ might be high. On the other hand, the calculation of the spin current with $\hat{j}_2 = \frac{d(\hat{r}\hat{s})}{dt}$ is rather involved in practice (although this definition looks simple). To the best of our knowledge, this definition has only been applied in simple model systems, and to the linear order responses.

Here we roughly estimate the difference between the spin current defined with $\hat{j}_1 = \frac{1}{2}(\hat{v}\hat{s} + \hat{s}\hat{v})$ and $\hat{j}_2 = \frac{d(\hat{r}\hat{s})}{dt}$. Compared with \hat{j}_1 , \hat{j}_2 has an additional term that comes from the torque on the spins [*PRL* **96**, 076604 (2006), see also *PRL* **97**, 236805 (2006)]. This term is proportional to $[\hat{H}, \hat{s}]$. Therefore, the relative difference $\left| \frac{\hat{j}_2 - \hat{j}_1}{\hat{j}_1} \right|$ can be roughly estimated from $\alpha_i \equiv \frac{\|[\hat{H}, \hat{s}^i]\|}{\|\hat{H}\| \cdot \|\hat{s}^i\|}$,

where $\|\cdot\|$ indicates matrix norm¹. We have thus calculated and plotted α_z in the first Brillouin zone for MoS₂ (Figure R1a) and MnBi₂Te₄ (Figure R1b). One can see that α_z is on the order of 0.1 ~ 0.2. From this point of view, one may deduce that the difference between \hat{j}_1 and \hat{j}_2 is indeed not negligible, but in general cases, it would not qualitatively change the main results.

As described above, \hat{j}_2 is not a perfect definition of spin current in the presence of external light, either. It might be possible to find a better definition of the spin current that is conserved even when the system is under light illumination. But this is beyond the scope of the current work, and we would like to leave this for future work.

In the first paragraph on page 6 of the main text, we added,

“We would like to remark that there are lots of debates on the definition of spin current⁴⁰⁻⁴², see SM for detailed discussions.”

Detailed discussions above, including Figure R1, have been added in the Supplementary Materials.

3) What are the employed assumptions for loss mechanisms of pure spin photocurrents? For example, in a simple situation analyzed in 1) in addition to the spin relaxation, the spin current can be lost through carrier recombination. This spin dynamics and spin-orbit coupling for electrons and holes are inequivalent.

Reply: We thank the reviewer for these insightful comments. The loss of the spin photocurrents should come from the scattering with phonons, etc., which leads to the recombination of electron-hole (e-h) pairs. As also pointed out by reviewer #1, the shift mechanism comes from the fact that the electron-hole pair has non-zero electric dipole p in non-centrosymmetric materials. However, such dipole would be lost when the electron and hole recombine. Assuming an e-h pair generation rate of R , and a scattering/recombination time of τ , then the steady-state polarization is $P = Rp\tau$. The current, which is the polarization generation rate, can be obtained

¹ This can be naively understood in the following way. We have $\hat{j}_2 = \frac{d(\hat{r}\hat{s})}{dt} = \frac{d\hat{r}}{dt}\hat{s} + \hat{r}\frac{d\hat{s}}{dt} = \frac{1}{2}\{[\hat{H}, \hat{r}], \hat{s}\} + \frac{1}{2}\{\hat{r}, [\hat{H}, \hat{s}]\}$, where $\{a, b\} = ab + ba$ ensures hermiticity. The first term is just \hat{j}_1 , while the second term comes from the torque on the spins. The ratio between these two terms is (very roughly) $\frac{\|[\hat{H}, \hat{s}]\|}{\|\hat{H}\| \cdot \|\hat{s}\|}$. Rigorously speaking, the position operator \hat{r} needs extra care in infinite solid-state systems.

from $j \propto \frac{P}{\tau} = Rp$, and is independent of τ . On the other hand, the injection mechanism comes from the different velocities of electrons and holes, which is $\Delta_{eh} = v_{ee} - v_{hh}$. The velocity difference leads to a current of $j \propto \rho \Delta_{eh}$, where $\rho = \tau R$ is the steady-state e-h density. Thus, the injection current conductivity is linearly dependent on τ . Some more discussions can be found in our reply to the 6th comment of Reviewer #1 (on page 10-11 of this document).

One can see that both the shift and injection mechanism are dependent on the scattering processes of the electrons and holes. Usually, the scattering time τ is on the order of sub-picoseconds. On the other hand, the spin relaxation time is usually longer, on the order of (sub-)nanoseconds. For example, in [*Nat. Phys.* **11**, 830 (2015)] it was shown that TMD has a spin relaxation time on the order of ns. Similar arguments can also be found in [*Appl. Phys. Lett.* **80**, 1558 (2001), *Nat. Comm.* **4**, 2068 (2013), etc.]. Thus, usually the main loss mechanism should be the scattering of electrons/holes, which leads to the momentum relaxation and the recombination of e-h pairs. Of course, in some cases, the spin relaxation time may be shorter (for example, holes usually have shorter spin relaxation time, and the spin relaxation time may be shorter in the presence of magnetic impurities.). In these cases, we are in a different regime and the spin relaxation would be the main loss mechanism. Approximately, one may expect that $\frac{1}{\tau} = \frac{1}{\tau_{\text{scattering}}} + \frac{1}{\tau_{\text{relaxation}}}$, where $\tau_{\text{scattering}}$ is the e/h scattering time, while $\tau_{\text{relaxation}}$ is the spin relaxation time.

Regarding the difference spin dynamics of electrons and holes, we note that in principle τ should not be a constant, but varies with different band n and wavevector k . The difference between electrons and holes shall be included by using a mode-dependent τ . More rigorously, one should use $\frac{\partial \rho}{\partial t} |_{\text{coll}}$ that includes scatterings, spin dynamics, etc., in the von Neumann equation (Eq. S4 in the Supplementary Materials). One has

$$\frac{\partial \rho}{\partial t} = -\frac{i}{\hbar} [H, \rho] + \frac{\partial \rho}{\partial t} |_{\text{coll}} \quad (2)$$

However, for convenience, we adopt the constant relaxation time approximation and use $\frac{\partial \rho}{\partial t} |_{\text{coll}} \approx -\frac{\rho - \rho_0}{\tau}$. We would like to remark that including these subtleties would not change the essence of the results in our work.

In the last paragraph on page 7 of the main text, we added,

“The main dissipation mechanism here is the scattering of electrons and holes with e.g., phonons. The scattering time τ is usually on the order of (sub)-picoseconds. In some cases, when the spin relaxation time is short, it can be the main loss mechanism as well. Also, in the presence of scattering potentials (from e.g., impurities), there could be skew scattering and side jump, which lead to extrinsic spin/charge currents, as compared with the intrinsic currents discussed in this work, which originates in the intrinsic band structure. Another point we would like to mention is that, here we adopt the constant relaxation time approximation and use a constant τ for all modes (band index n and wavevector k). But in reality, τ should be mode-dependent. (see SM for more discussions)”

Detailed discussions above are added in the Supplementary Materials.

4) Perhaps some clarification for the points above could be given by moving the p.15 comment about focusing only on intrinsic currents to an earlier place in the manuscript. Even in such intrinsic regime, how can one understand the corresponding time/length scales for the presence of spin photocurrents?

Reply: We thank the reviewer for these helpful comments. As discussed above, the shift and injection mechanisms rely on the fact that electrons and holes carry different spins and velocities. Such a process would stop once the electrons or holes scatter and recombine. Thus, the relevant time scale here should be the scattering time τ , which is usually on the sub-picosecond scale. Regarding the length scale, the group velocities of electrons and holes are usually on the order of $v = 10^5 \sim 10^6$ m/s. Thus, the length scale here should be $l = v\tau$, which on the order of tens of nanometers. This should be compared with the mechanism based on junctions, as presented in [*Appl. Phys. Lett.* **80**, 1558 (2001), *Nat. Comm.* **4**, 2068 (2013)]. In these works, the electrons and holes move diffusively, and the relevant length scales are relatively larger, on the order of micrometers.

We have moved the discussions on page 15 to page 7 of the revised manuscript, as shown in our reply to the previous question.

5) For an experimental detection of spin photocurrent, could one use spin extraction [predicted in Phys. Rev. Lett. and measured in Nat. Comm. noted above]?

Reply: We thank the reviewer for these comments. In our understanding, spin injection and extraction describe the following processes. A nonmagnetic semiconductor forms a junction with magnetic material. When the carriers flow from the magnetic material to the nonmagnetic semiconductor, they can be spin-polarized, because there are a different number of spin up and down carriers in the magnetic material. This process is dubbed “spin injection” since the spin polarization is kind of “injected” into the semiconductors from the magnetic material. On the other hand, carriers originally in the semiconductor can also flow into the magnetic material. During this process, spin up and down carriers have different probabilities to enter the magnetic materials. This is somewhat similar to the giant magnetoresistance effect. It was also pointed that either the spin up or spin down carriers can have a higher probability to enter the magnetic materials, depending on the actual condition of the junction [*Science* **309**, 2191 (2005), *PRL* **98**, 046602 (2007)]. If the spin up (down) electrons have a higher probability to enter the magnetic materials, then the semiconductor will be left spin down (up), and thus becomes spin-polarized. This process is dubbed “spin extraction” since the spin polarization is kind of “extracted” from the magnetic materials.

We believe that a similar mechanism can be used to detect the spin photocurrent. We can consider a heterojunction using MoS₂ with a ferromagnetic material. When we shine light on MoS₂, a spin current will be generated. The carriers will tunnel into the magnetic material and lead to a current in it. This current would have a different magnitude if the magnetic moment of the magnetic material is parallel or anti-parallel to that of the spin current. We can monitor this effect by switching the magnetic moment with an external magnetic field, or switching the spin polarization of the spin photocurrent by using a light with different polarization (see Figure 2e of the main text). However, it might be improper to call this effect “spin extraction”. Because spin extraction describes a process that the carriers in a semiconductor become spin-polarized *because of* the junction with magnetic materials. But for the process described above, the electrons in the semiconductor are already spin-polarized before entering the magnetic materials.

6) References are not given in a uniform style. Some journal names are abbreviated, some not. Ref. 10 has typos and repeated authors, extra number appear in Ref. 27, 45, 67. Are Refs. 31, 40, 47 complete?

Reply: We thank the reviewer for these careful observations. We have carefully checked all our references, and manually edited the incorrect renderings of the Mendeley plugin.

This manuscript describes an important opportunity to realize spin photocurrent in a wide range of materials. Following these clarifications, it will be easier to assess its suitability for a broad readership and a publication in Nature Communications.

Reply: We thank the reviewer again for these positive and encouraging comments. We hope that we have appropriately addressed the comments of the reviewer.

Reviewers' Comments:

Reviewer #1:

Remarks to the Author:

Dear Editors,

The manuscript titled "Pure spin photocurrent in non-centrosymmetric crystals: bulk spin photovoltaic effect" has been revised by the authors in response to the comments from both referees. With their response, the authors have addressed most of the main concerns of the referees. Specifically, I am now convinced that their conclusion that "nonlinear optical (NLO) effect can be used to generate pure spin currents" "if the system possesses additional mirror symmetry or inversion-mirror symmetry" is novel and interesting enough to be published in Nature Communication.

In reviewing the background, I only noticed one issue in the introduction. The following paper PHYSICAL REVIEW B 95, 224430 (2017) discusses spin currents in inversion broken but time-reversal preserving spin photocurrents at second order in electric field. This appears quite relevant to the current manuscript and should be cited. However, I agree with the authors that pure spin-currents haven't been discussed.

Apart from this change, I would recommend publication in Nature Communication.

Reviewer #2:
Remarks to the Author:

The authors have provided a balanced and detailed response to both reviewers and made related changes in the main text and Supplementary Information. These changes and additional calculations now provide more accurate statements. For example, it was helpful to downplay the low-dissipation aspect of pure spin currents, improve the symmetry arguments, clarify the novelty of the work, or explain possible loss mechanisms for pure spin current.

Even with these changes one can argue (and the authors mention that) that the fully accurate picture of the underlying phenomena is not yet available. In realistic systems with spin-orbit coupling there remain subtleties about the definition of the spin current. This is mentioned in Ref. 41 and the changes with different definition of spin current are further explored in the present work, including new Fig. S1. Additionally, Ref. 41 notes that there are subtleties in spin currents with the choice of boundary conditions, mentioning an example in spin Hall effect [PRB 72, 241303(R), (2005)], which may also pertain to the present work due to nonuniform illumination or spatially-dependent absorption. However, in the revised manuscript what the authors present about the description of spin current already matches the current state-of-the-art and I expect will provide a valuable guidance for a broad readership interested in studies of nonlinear optical effects in a growing number of materials. Therefore, while the knowledge of spin current will continue to evolve, these findings are likely to motivate both emerging applications and probing surface-state properties of topological materials.

With the interest in verifying these predictions, it may help to discuss more when this picture will break down. For example, at the level of a simple estimate as given in Eqs. (R1)- (R3) and using MoS₂ parameters, what is the maximum magnitude of spin current? Will the predicted NLO behavior qualitatively change with an increase in illumination, or the sample will first be destroyed? These estimates can serve as a guidance analogous to gate-controlled effects in spintronics, which are limited by the characteristic breakdown fields and thus limit the generated excess carrier density.

I expect that the implications of these findings to get intriguing effects from light illumination will become relevant in a growing number of materials. I recommend this manuscript for a publication in Nature Communications.

Reply to Reviewers

Reviewer #1:

The manuscript titled "Pure spin photocurrent in non-centrosymmetric crystals: bulk spin photovoltaic effect" has been revised by the authors in response to the comments from both referees. With their response, the authors have addressed most of the main concerns of the referees. Specifically, I am now convinced that their conclusion that "nonlinear optical (NLO) effect can be used to generate pure spin currents" "if the system possesses additional mirror symmetry or inversion-mirror symmetry" is novel and interesting enough to be published in Nature Communication.

Reply: We thank the reviewer for reviewing our paper again and for all these encouraging comments.

In reviewing the background, I only noticed one issue in the introduction. The following paper PHYSICAL REVIEW B 95, 224430 (2017) discusses spin currents in inversion broken but time-reversal preserving spin photocurrents at second order in electric field. This appears quite relevant to the current manuscript and should be cited. However, I agree with the authors that pure spin-currents haven't been discussed.

Reply: We thank the reviewer for pointing out this relevant paper. We have cited this paper in our introduction as Ref. 28,

“Alternatively, a spin current can be generated with a mechanism reminiscent of the p-n junction in solar cells^{23–25}, quantum interference^{26,27}, or the nonlinear Drude current²⁸.”

Apart from this change, I would recommend publication in Nature Communication.

Reply: We thank the reviewer for recommending the publication of our paper.

Reviewer #2:

The authors have provided a balanced and detailed response to both reviewers and made related changes in the main text and Supplementary Information. These changes and additional calculations now provide more accurate statements. For example, it was helpful to downplay the low-dissipation aspect of pure spin currents, improve the symmetry arguments, clarify the novelty of the work, or explain possible loss mechanisms for pure spin current.

Reply: We thank the reviewer for reviewing our paper again and for all these encouraging comments.

Even with these changes one can argue (and the authors mention that) that the fully accurate picture of the underlying phenomena is not yet available. In realistic systems with spin-orbit coupling there remain subtleties about the definition of the spin current. This is mentioned in Ref. 41 and the changes with different definition of spin current are further explored in the present work, including new Fig. S1. Additionally, Ref. 41 notes that there are subtleties in spin currents with the choice of boundary conditions, mentioning an example in spin Hall effect [PRB 72, 241303(R), (2005)], which may also pertain to the present work due to nonuniform illumination or spatially dependent absorption. However, in the revised manuscript what the authors present about the description of spin current already matches the current state-of-the art and I expect will provide a valuable guidance for a broad readership interested in studies of nonlinear optical effects in a growing number of materials. Therefore, while the knowledge of spin current will continue to evolve, these findings are likely to motivate both emerging applications and probing surface-state properties of topological materials.

Reply: We thank the reviewer for these careful and insightful observations. Indeed, the definition of the spin current remains an issue to be explored and is attracting research interest until today. We will study these issues in future works.

With the interest in verifying these predictions, it may help to discuss more when this picture will break down. For example, at the level of a simple estimate as given in Eqs. (R1)- (R3) and using MoS2 parameters, what is the maximum magnitude of spin current? Will the predicted

NLO behavior qualitatively change with an increase in illumination, or the sample will first be destroyed? These estimates can serve as a guidance analogous to gate-controlled effects in spintronics, which are limited by the characteristic breakdown fields and thus limit the generated excess carrier density.

Reply: We thank the reviewer for these insightful comments. With MoS₂ parameters, when the external field strength is $E = 1 \text{ MV/m}$, the spin current density is $10^8 \frac{\text{A}}{\text{m}^2} \frac{\hbar}{2e}$, and the temperature rise in the sample is estimated to be on the order of 1 K, which is not high. If we further increase the electric field strength, then two main issues will arise. 1) On the experimental side, a strong laser may destroy the sample, as pointed by the reviewer. This might happen for electric field strength above 10 MV/m when one uses a continuous wave laser. In this case, the spin current density is around $10^{10} \frac{\text{A}}{\text{m}^2} \frac{\hbar}{2e}$, which is quite high, while the temperature rise can be as high as 100 K. Note that the temperature rise can be mitigated with better thermal management. Also, the sample may survive in an even stronger electric field if a pulsed laser is used. For example, with a femtosecond laser, the electric field can be as high as 100 MV/m, with a temperature rise of 10 K. 2) On the theoretical side, the perturbation theory used in the current work may fail when the electric field is too strong. The external electric field strength should be compared with the intrinsic interaction strength in the materials, which is usually on the order of $1 \frac{\text{V}}{\text{\AA}} = 10^4 \frac{\text{MV}}{\text{m}}$. From this point of view, the perturbation theory may work up to an electric field strength of 100 MV/m. Above this strength, the error from perturbative expansions may not be ignored and non-perturbation theories may be required.

In summary, with a pulsed laser, our theoretical picture may work up to an electric field strength up to 100 MV/m, when the spin current density is on the order of $10^{12} \frac{\text{A}}{\text{m}^2} \frac{\hbar}{2e}$. This is restricted by both experimental (sample damage) and theoretical (validity of perturbation theory) concerns. With a continuous wave laser, one may have to use an electric field strength below 10 MV/m to keep the temperature rise and sample damage manageable. At this field strength, the spin current density can be $10^{10} \frac{\text{A}}{\text{m}^2} \frac{\hbar}{2e}$ with the monolayer MoS₂ parameters.

We have added the discussions above in the Supplementary Materials.

I expect that the implications of these findings to get intriguing effects from light illumination will become relevant in a growing number of materials. I recommend this manuscript for a publication in Nature Communications.

Reply: We thank the reviewer again for these positive comments and the recommendation for the publication of our paper.